Ultraluminous X-Ray Sources in Nearby Galaxies from Rosat HRI Observations. II. Statistical Properties

Ji-Feng Liu – University of Michigan

Joel N. Bregman – University of Michigan

Jimmy Irwin – University of Michigan

Citation of published version:

Liu, J., Bregman, J., Irwin, J. (2006): Ultraluminous X-Ray Sources in Nearby Galaxies from Rosat HRI Observations. II. Statistical Properties. *The Astrophysical Journal*, 642(1). DOI: 10.1086/500787

The Astrophysical Journal, 642:171–187, 2006 May 1

ULTRALUMINOUS X-RAY SOURCES IN NEARBY GALAXIES FROM *ROSAT* HRI OBSERVATIONS. II. STATISTICAL PROPERTIES

Ji-Feng Liu, Joel N. Bregman, and Jimmy Irwin
Astronomy Department, University of Michigan, MI 48109
Received 2005 May 20; accepted 2005 December 22

ABSTRACT

The statistical properties of the nonnuclear X-ray point sources from the *ROSAT* HRI survey of nearby galaxies in Paper I are studied, with particular attention to the contamination from background and/or foreground objects. This study reveals a statistical preference for the ultraluminous X-ray sources (ULXs) to occur in late-type galaxies over early-type galaxies, and in starburst/H II galaxies over nonstarburst galaxies. There is a trend of greater occurrence frequencies and ULX rates for galaxies with increasing star formation rates, confirming the connection between the ULX phenomenon and the star formation. A nonlinear correlation is found between the number of ULXs and the star formation rate, with significantly more ULXs at low star formation rates than the ULX population expected from the high-mass X-ray binaries (HMXBs) as an indicator of the star formation and the accompanying young stellar population, suggestive of another population of ULXs associated with the low-mass X-ray binaries (LMXBs) and the old stellar population. There are no breaks around 10^{39} ergs s^{-1} in the luminosity functions of ULXs in all galaxies or in late-type galaxies, suggesting the regular ULXs below 10^{40} ergs s^{-1} are a high-luminosity extension of the ordinary HMXB/LMXB populations below 10^{39} ergs s^{-1}. There is evidence that the extreme ULXs above 10^{40} ergs s^{-1} might be a different ULX class from the regular ULXs below 10^{40} ergs s^{-1}, although a larger sample with more ULXs is needed to establish the statistical properties of the extreme ULXs as a class.

Subject headings: catalogs — galaxies: general — X-rays: binaries — X-rays: galaxies

1. INTRODUCTION

Ultraluminous X-ray sources (ULXs) are extranuclear point sources with luminosities in the range of 10^{39}–10^{41} ergs s^{-1}, and have been observed by the *Einstein Observatory* (e.g., Fabbiano 1989), *Röntgensatellit* (*ROSAT*; e.g., Colbert & Mushotzky 1999), and *Advanced Satellite for Cosmology and Astrophysics* (*ASCA*; e.g., Makishima et al. 2000), and recently by the *Chandra* and *XMM-Newton* X-ray observatories in many galaxies (e.g., Kilgard et al. 2002; Swartz et al. 2004). As compared to the cases of the X-ray binaries in our Galaxy, which are powered by accretion onto neutron stars or stellar mass black holes and have luminosities of 10^{33}–10^{39} ergs s^{-1}, the luminosities of ULXs require accreting black holes of masses 10^2–10^4 $M_\odot$ if they emit at 0.1–0.01 of the Eddington luminosity, typical of Galactic X-ray binaries (Colbert & Mushotzky 1999). Such intermediate-mass black holes, if they exist, bridge the gap between stellar mass black holes and supermassive black holes of 10^6–10^9 $M_\odot$ in the center of galaxies. Alternatively, ULXs could be stellar mass black holes or neutron stars whose apparent super-Eddington luminosities are due to some special processes. One suggestion is that radiation-pressure–dominated accretion disks with photon-bubble instabilities are able to emit truly super-Eddington luminosities (Begelman 2002). Another suggestion is that beaming effects can produce the observed luminosities of ULXs (King et al. 2001).

The leading goals in ULX studies are to determine the masses of the primary, to understand how and where they form, and to find out how they emit at such high luminosities. In the last few years, observations of many ULXs in nearby galaxies have been made to address these questions, and important clues have been revealed on their spectra (e.g., Makishima et al., 2000; Miller et al. 2003; Kong et al. 2004), their preferential occurrence in galaxies with current star-forming activities (e.g., Kilgard et al. 2002; Zezas et al. 2002; Gao et al. 2003), their short-term and long-term variabilities, periodic variations (e.g., Sugiho et al. 2001; Bauer et al. 2001; Liu et al. 2002a), and quasi-periodic oscillations (e.g., Strohmayer & Mushotzky 2003; Soria et al. 2004; Soria & Motch 2004; Liu et al. 2005). Aside from in-depth studies of some well-known ULXs, the study of a complete sample of ULXs, with incompleteness carefully calculated, is necessary to study the defining properties of ULXs as a class, and to calculate the occurrence rates and luminosity functions that will place constraints on models for how ULXs form and evolve.

With observations of individual ULXs in nearby galaxies accumulating, now it is becoming feasible to construct samples with a statistically significant number of ULXs. So far there are only a few such studies. Colbert & Ptak (2002, hereafter CP2002) analyzed 1883 High Resolution Imager (HRI) observations to search for ULXs in galaxies with $cz < 5000$ km s^{-1} in the *Third Reference Catalog of Galaxies* (de Vaucouleurs et al. 1991, hereafter RC3). They found 87 ULXs in 54 galaxies, with 37 in early-type galaxies. Based on this catalog, Ptak & Colbert (2004) found that ~12% of galaxies contain at least one ULX with $L_X \geq 10^{39}$ ergs s^{-1} and ~1% of galaxies contain at least one ULX with $L_X \geq 10^{40}$ ergs s^{-1} in 2–10 keV. However, many ULXs in the CP2002 catalog are projected far from the host galaxies, and they may be foreground stars or background active galactic nuclei (AGNs) or QSOs instead (Irwin et al. 2004). Recently Swartz et al. (2004) analyzed the archive *Chandra* ACIS observations for 82 nearby galaxies, in which they found 154 nonnuclear point sources with $L_X \geq 10^{39}$ ergs s^{-1} in 0.5–8 keV as ULX candidates. They estimate a ULX rate of 1.5 ± 0.55 (0.55 ± 0.10) ULXs per 10^{10} $M_\odot$ for spiral (elliptical) galaxies, with a false ULX percentage of 14% (44%) from the background QSOs/AGNs.

We have carried out a survey of ULXs in nearby galaxies with *ROSAT* HRI archival data (Liu & Bregman, 2005, hereafter Paper I), which takes advantage of the moderate spatial resolution of HRI (an on-axis FWHM of $<5''$) and the large sky coverage (~2%) of the data archive. This survey encompasses 313 galaxies

within 40 Mpc with isophotal diameters >1′ observed by 467 HRI observations, with an average of 2.2 observations per galaxy. Uniform data reduction procedures were applied to all observations to detect point sources with a wavelet detection algorithm, for which simulations were run to understand its behavior on HRI observations, including false detection rates, detection thresholds, and correction factors to correct detected counts to true source counts based on the detection significance and the off-axis angles of detected sources. As a result, 106 extranuclear point sources with $L_X \geq 10^{39}$ ergs s^{-1} in 0.3–8 keV (defined as ULX candidates) are found within the D_{25} isophotes of 63 galaxies, with 10 already identified as QSOs or stars. There are 110 ULX candidates found between $1D_{25}$ and $2D_{25}$ of 64 galaxies, with 16 already identified as QSOs or stars.

To minimize the contamination from background and/or foreground objects, in Paper I we constructed a clean sample of 109 ULXs from the ULX candidates by selecting only those within the D_{25} isophotes or with apparent connections with the host galaxy (e.g., along spiral arms), and excluding those identified as QSOs and stars. The trend that ULXs are preferentially found in spiral galaxies is clearly shown in the clean sample, with 49 out of 181 spiral galaxies in our survey hosting 89 ULXs, while 4 out of 93 early-type galaxies host seven ULXs if we exclude the eight ULXs in two peculiar lenticular galaxies NGC 1316 and NGC 5128. However, it is inappropriate to compute the occurrence frequency of ULXs in spiral (early-type) galaxies with this clean sample, because the selection criteria for ULXs in this sample are not uniform, and the contamination from background and foreground objects, although small, is uncertain.

In this paper we compute the ULX rates and the luminosity functions of ULXs in different types of galaxies with the contamination carefully calculated and subtracted. In § 2 we present the methodology used in our analysis, including how ULX samples are constructed from the HRI survey, how the contamination is calculated, what aspects of the samples are studied, and how the ULX rates are normalized by the surveyed blue light. We compare in § 3 the statistical properties of ULX samples in different types of galaxies, including early-type galaxies, late-type galaxies, starburst and nonstarburst galaxies, and galaxies with different star formation rates. We study the radial distribution of ULXs with respect to the isophotal ellipses of the galaxies in § 4. In § 5 we compare our results to similar works, and their implications on the nature of ULXs.

2. METHODOLOGY

Statistical analysis of large samples of ULXs is essential for studying ULXs as a class. There have been a few such studies, e.g., CP2002, Kilgard et al. (2002), Ptak & Colbert (2004), and Swartz et al. (2004). Here we present our method for analyzing the ULX samples from our *ROSAT* HRI survey, with particular care on the contamination problem.

2.1. *Construction of ULX Samples*

The total HRI survey includes 313 galaxies of different types with different properties. In our study, we divide the 313 galaxies into groups to study the connection between ULXs and the properties of the galaxies. Galaxies are grouped based on the morphological types of the galaxies to reveal possible trends of ULXs along the Hubble sequence. To study the connection between the star formation activities and the ULX phenomenon, we group the galaxies based on whether they are starburst or H II galaxies, and also based on the star formation rates calculated from the far-infrared luminosities.

A complete ULX sample is extracted from a snapshot survey of galaxies, in which a galaxy is observed in *one* observation, by selecting *all* nonnuclear X-ray point sources within (parts of) the galaxies with $L_X \geq 10^{39}$ ergs s^{-1}. Such a sample is an instantaneous sample, which is different from the collection of ULX candidates from all 313 survey galaxies listed in Table 3 of Paper I, because the latter is collected from *multiple* observations of galaxies. Such a sample is also different from the clean sample of ULXs defined in Paper I, because some nonnuclear sources identified as background QSOs and foreground stars are excluded from the clean sample.

To make a snapshot survey of the galaxies, one observation needs to be selected for each galaxy. One way is to select the observation with the longest exposure for each galaxy, which we refer as the deep survey. Another way is to select a random observation from all available for each galaxy to form a random survey. In our analysis, we compute 20 random surveys, the average of which is calculated and referred as the average survey. The ULX samples drawn from the average survey and the deep survey are slightly different, because the X-ray sources vary in luminosity between observations, and the deep survey has larger low-luminosity coverage than the average survey.

The ULX candidates are grouped by their proximity to the galactic center into those within the D_{25} isophotes, and those between $1D_{25}$ and $2D_{25}$. In our discussion, we focus on the statistical properties of the ULX samples within the D_{25} isophotes of the galaxies, which presumably have a higher percentage of "true" ULXs than the ULX samples between $1D_{25}$ and $2D_{25}$. To reveal how ULXs are distributed radially in galaxies, we study the ULX samples within annuli of the isophotes in § 4, and compare the ULX sample between $1D_{25}$ and $2D_{25}$ to the ULX sample within the D_{25} isophotes.

In the following subsections, we describe how we calculate the number of contaminating sources based on the $\log N - \log S$ relation, the surveyed blue light curve, the ULX rates, and luminosity functions for the ULX samples.

2.2. *Contamination of ULX Samples*

ULXs are usually defined by associating an X-ray source to a galaxy based on its projected proximity to the galaxy. Such a definition inevitably introduces into a ULX sample the contamination from foreground and/or background objects, which must be excluded when studying the statistical properties of the ULX sample. A direct way is to make deep optical and/or spectroscopic observations of every ULX candidate in a sample, identify and exclude those foreground and/or background objects. However, it is impractical to make such studies for all ULXs in a large sample, considering the huge amount of telescope time needed, although optical and spectroscopic studies of prime examples of ULXs are essential and have to be made to determine the nature of the ULX systems.

A practical way to estimate the contamination from background and foreground objects, as used in this paper, is to make predictions from the $\log N - \log S$ relation and exclude the predicted numbers from the ULX sample in the statistical studies that follow. For the HRI observations in this survey, it is appropriate to use the $\log N - \log S$ relation derived from *ROSAT* observations (Hasinger et al. 1998), where the differential form is $dN/dS = N_1 S^{-\beta_1}$ for $S > S_b$ and $dN/dS = N_2 S^{-\beta_2}$ for $S < S_b$, with S in units of 10^{-14} ergs s^{-1} cm^{-2}, $S_b = 2.66 \pm 0.66$, $N_2 = 111 \pm 10$, $\beta_1 = 2.72 \pm 0.27$, $\beta_2 = 1.94 \pm 0.19$, and $N_1 = 238.1$. With this differential relation, the number of contaminating sources in a flux interval can be calculated with the survey area curve $A(>S)$ that gives the area (i.e., solid angle) in which

sources brighter than the limiting flux S can be detected in the survey. We estimate a typical error of 10% for the predicted number of contaminating sources, and a higher error of up to 20% for fainter sources.

The survey area curve $A(>S)$ can be calculated for an observation given the sensitivity (detection threshold) of the observation. For our data reduction procedures, the 3 σ detection threshold can be computed with the background level and the source size that has been derived from simulations in Paper I as a function of the off-axis angle θ. A sensitivity map is constructed for each observation by computing the detection thresholds (in units of counts s^{-1}) at the location of every pixel, with the average background level computed from the part of the detector with off-axis angle $\theta < 17'$ excluding the detected sources. The survey area curve $A(>S)$ for a galaxy in this observation can be computed by summing up the area of the pixels within this galaxy for which the detection thresholds correspond to flux less than S. Similarly, the survey area curves for parts of a galaxy, e.g., the region between $1D_{25}$ and $2D_{25}$, can be computed by considering only pixels within those parts. In the computation, the $10''$ nuclear region for a galaxy is excluded.

The detection threshold in count rate is converted to flux S by assuming a power-law spectrum, using Galactic H I column density toward the galaxy, with a photon index of 2 within 0.5–2.4 keV to be consistent with what was used in the derivation of the $\log N - \log S$ relation (Hasinger et al. 1998). Note that the flux S for use in the $\log N - \log S$ relation is different from the apparent flux F, used to calculate the luminosity L in Paper I, because for the flux F we used a power-law spectrum with a photon index of 1.7 within 0.3–8.0 keV to be comparable to *Chandra* observations. The flux F is higher than S by a factor of $\sim$3 for the same count rate, with the factor varying slightly with the Galactic H I column density used in the conversions.

Given the survey area curve $A(>S)$ for a galaxy in an observation, the number of background and foreground objects can be calculated by integrating the product of dN/dS and $A(>S)$ over flux intervals. The number $N_b(S_1, S_2)$ over a flux interval of (S_1, S_2) is

$$N_b(S_1, S_2) = \int_{S_1}^{S_2} \frac{dN}{dS} A(>S)\, dS.$$

To estimate the number $N_b(L_1, L_2)$ for a galaxy in an apparent luminosity bin (L_1, L_2), the luminosity L is converted to S using a function $S_g(L)$ with the distance to the galaxy, and with proper consideration of the different conversion factors from the count rate to flux S and flux F. For a group of galaxies, the total number $N_b(L_1, L_2)$ can be calculated by summing up the numbers for individual galaxy in their respective observation, i.e.,

$$N_b(L_1, L_2) = \sum_g \int_{S_g(L_1)}^{S_g(L_2)} \frac{dN}{dS} A_g(>S)\, dS.$$

Here $S_g(L)$ has a dependence on the distance of the galaxy and the Galactic H I column density toward the galaxy.

2.3. *Blue Light Surveyed in ULX Surveys*

The occurrence rates of ULXs in different types of galaxies place constraints on models on how ULXs form and evolve. The occurrence rate can be directly calculated as the number of ULXs per galaxy, or calculated as the number of galaxies per unit of stellar mass to account for the variations in the size and stellar mass of galaxies among and within different types. The stellar mass content of a galaxy can be inferred from the total light of the galaxy with the stellar mass-to-light ratio. While the mass-to-light ratios have larger variations in the optical than in the near-infrared (Bell & De Jong 2001), in our analysis we use the blue light from RC3 and calculate the number of ULXs per $10^{10}\, L_\odot$ of blue light, due to the lack of a uniform compilation of near-infrared magnitudes for the survey galaxies.

The surveyed blue light curve $\mathcal{L}_g(L)$ for a galaxy gives the blue light of the stellar contents in which X-ray sources above L can be detected in an observation. To compute the detection threshold in L, we calculate the detection threshold in count rate for each pixel of the HRI image as described in § 2.2, convert it to flux F by using a power-law spectrum with a photon index of 1.7 in 0.3–8 keV, and calculate $L = 4\pi D^2 F$ with D as the distance to the galaxy. To compute the blue light, we compute the light profile for the galaxy from the total blue light $\mathcal{L}_B$ and the effective radius R_e that encloses 50% of the total light. For two-thirds of the survey galaxies, the effective radii are taken from RC3, with an average R_e of $0.15D_{25}$. For one-third of the survey galaxies without R_e from RC3, we assume $R_e = 0.15D_{25}$. The blue magnitudes of 297 survey galaxies are taken from the RC3 catalog and converted to blue light $\mathcal{L}_B$ in units of $L_\odot$ with $M_{B\odot} = 5.46$ mag.

The light profile for early-type galaxies is usually expressed by the de Vaucouleurs $R^{1/4}$ law, $I(R) = I_e 10^{3.33-3.33(R/R_e)^{1/4}}$. Here R is the elliptical radius, I_e is the surface brightness at the effective radius R_e, and the total light can be expressed as $7.22\pi R_e^2 I_e$. With R_e and $\mathcal{L}_B$ known, the light profile can be expressed as $I(R) = \left(\mathcal{L}_B/7.22\pi R_e^2\right) 10^{3.33-3.33(R/R_e)^{1/4}}$.

The light profile for late-type galaxies is decomposed into a de Vaucouleurs bulge in the form of $I(R) = I_e 10^{3.33-3.33(R/r_e)^{1/4}}$, and an exponential disk in the form of $I(R) = I_0 e^{-R/h}$, with h as the scale height, I_0 as the surface-brightness at the galactic center, and the total light from the disk as $2\pi h^2 I_0$. The relative prominence of the two components change with the Hubble type T, and the bulge-to-disk (B/D) ratios, taken from Graham (2001) and interpolated when necessary, change from 25% at $T = 0$ to 1% at $T = 10$, with a general decrease toward later galaxy types. In spite of the variation in bulge-to-disk ratios, the r_e/h ratio is found to be quite constant, and we take $r_e/h = 0.2$ following Graham (2001). By assuming the effective radius R_e derived from RC3 encloses 50% of the disk light, we find $h = R_e/1.7$, $r_e = R_e/8.5$. This assumption is reasonable for most of the survey galaxies for which $B/D \ll 1$; for galaxies with nonnegligible bulges, this slightly overestimates r_e and h. Given $\mathcal{L}_B$ from RC3, we find $I_0 = [\mathcal{L}_B/(1 + B/D)]\left(1.7^2/2\pi R_e^2\right)$, and $I_e = [\mathcal{L}_B/(D/B + 1)]\left(8.5^2/7.22\pi R_e^2\right)$. With r_e, h, I_e, and I_0 calculated from R_e and $\mathcal{L}_B$, the light profile can be calculated with $I(R) = I_e 10^{3.33-3.33(R/r_e)^{1/4}} + I_0 e^{-R/h}$.

The surveyed blue light curve $\mathcal{L}_g(L)$ for a galaxy can be computed by summing up the blue light in pixels within the galaxy (with the $10''$ nuclear region excluded) for which the detection thresholds correspond to luminosities below L. Similarly, the curve $\mathcal{L}_g(L)$ for parts of a galaxy, e.g., the region between $1D_{25}$ and $2D_{25}$, can be computed by considering only pixels within those parts. The survey light curves $\mathcal{L}_g(L)$ are computed for (parts of) the 297 survey galaxies in different observations with the same procedures. The total survey light curve $\mathcal{L}(L)$ for a group of galaxies is computed by summing up the survey light curves of individual galaxies in their respective observations.

2.4. *Statistical Descriptions of ULX Samples*

With the contamination and the surveyed blue light computed for a survey, we study the statistical properties of the ULX

TABLE 1
ULX Occurrence Rates for Different Survey Galaxy Samples

Sample[a] (1)	$L_X \geq 10^{39}$ ergs s^{-1}[b]					$L_X \geq 1.6 \times 10^{39}$ ergs s^{-1}[c]				
	N_{SG}[f]	N_{HG}[g]	N_{HG}/N_{SG}[h]	N_U/N_{SG}[i]	N_U/N_{SG}[j]	N_{SG}[f]	N_{HG}[g]	N_{HG}/N_{SG}[h]	N_U/N_{SG}[i]	N_U/N_{SG}[j]
All	98	35	36 ± 6	1.71 ± 0.23	0.56 ± 0.09	131	33	25 ± 4.4	1.40 ± 0.21	0.32 ± 0.06
Early	22	1	4.5 ± 4.5	1 ± 1	0.023 ± 0.10	35	3	8.6 ± 4.9	1.07 ± 0.67	0.08 ± 0.09
Earlyx	21	1	4.8 ± 4.8	1 ± 1	−0.019 ± 0.10	33	2	6.1 ± 4.3	1.10 ± 0.85	0.036 ± 0.07
Late	76	34	45 ± 7.7	1.73 ± 0.23	0.72 ± 0.10	96	30	31 ± 5.7	1.43 ± 0.22	0.41 ± 0.07
Pec	3	0	0 ± 0	0 ± 0	−0.033 ± 0.33	3	0	0 ± 0	0 ± 0	−0 ± 0.33
Ellip	11	0	0 ± 0	0 ± 0	−0.155 ± 0.13	16	1	6.2 ± 6.2	1.20 ± 1.40	−0.006 ± 0.12
Lent	11	1	9.1 ± 9.1	1 ± 1	0.19 ± 0.15	19	2	11 ± 7.4	0.95 ± 0.70	0.15 ± 0.12
Lentx	10	1	10 ± 10	1 ± 1	0.12 ± 0.14	17	1	5.9 ± 5.9	1 ± 1	0.08 ± 0.08
Sa	11	3	27 ± 16	1.53 ± 0.73	0.53 ± 0.26	18	1	5.6 ± 5.6	1 ± 1	0.19 ± 0.13
Sb	23	12	52 ± 15	1.93 ± 0.42	1.01 ± 0.23	32	13	41 ± 11	1.44 ± 0.35	0.49 ± 0.14
Sc	29	17	59 ± 14	2.09 ± 0.36	1.10 ± 0.21	36	15	42 ± 11	1.72 ± 0.35	0.63 ± 0.14
Sd	22	9	41 ± 14	1.86 ± 0.47	0.78 ± 0.20	23	7	30 ± 12	1.40 ± 0.46	0.43 ± 0.14
Sm	20	7	35 ± 13	1.13 ± 0.40	0.29 ± 0.12	23	6	26 ± 11	1.15 ± 0.43	0.25 ± 0.10
Sbrst	26	18	69 ± 16	1.81 ± 0.32	0.98 ± 0.20	29	15	52 ± 13	1.37 ± 0.31	0.53 ± 0.14
nSbrstL	52	16	31 ± 7.7	1.65 ± 0.34	0.56 ± 0.12	70	15	21 ± 5.5	1.51 ± 0.33	0.34 ± 0.08
SFRU	13	3	23 ± 13	1.30 ± 0.67	0.15 ± 0.11	18	2	11 ± 7.9	1.50 ± 0.85	0.16 ± 0.09
SFRA	18	6	33 ± 14	0.98 ± 0.40	0.24 ± 0.12	20	6	30 ± 12	0.98 ± 0.40	0.23 ± 0.11
SFRB	20	6	30 ± 12	0.98 ± 0.40	0.21 ± 0.11	22	6	27 ± 11	0.98 ± 0.40	0.21 ± 0.10
SFRC	17	7	41 ± 16	1.76 ± 0.51	0.84 ± 0.23	17	5	29 ± 13	1.76 ± 0.60	0.65 ± 0.21
SFRD	20	9	45 ± 15	1.59 ± 0.43	0.69 ± 0.20	24	7	29 ± 11	1.53 ± 0.47	0.42 ± 0.15
SFRE	13	7	54 ± 20	2.27 ± 0.59	1.19 ± 0.32	20	7	35 ± 13	1.50 ± 0.47	0.35 ± 0.16
SFRF	20	12	60 ± 17	2.38 ± 0.47	1.58 ± 0.30	26	11	42 ± 13	1.54 ± 0.38	0.67 ± 0.18
SFRG	18	13	72 ± 20	1.97 ± 0.41	1.37 ± 0.30	24	13	54 ± 15	1.45 ± 0.35	0.75 ± 0.19
SFRH	5	4	80 ± 40	1.52 ± 0.65	0.62 ± 0.40	8	4	50 ± 25	1.60 ± 0.65	0.62 ± 0.30

[a] The survey galaxy groups based on galaxy types, presence of starburst, and star formation rates (SFR). An "x" is suffixed when the two peculiar lenticulars, NGC 1316 and NGC 5128, are excluded from the early-type and lenticular galaxy groups.
[b] For ULXs with $L_X \geq 10^{39}$ ergs s^{-1}.
[c] For ULXs with $L_X \geq 1.6 \times 10^{39}$ ergs s^{-1}.
[d] For ULXs with $L_X \geq 4.0 \times 10^{39}$ ergs s^{-1}.
[e] For ULXs with $L_X \geq 10^{40}$ ergs s^{-1}.
[f] The number of galaxies with survey light $\geq$0.1 times its total light.
[g] The number of galaxies with at least 0.5 net ULXs.
[h] The percentage (%) of survey galaxies that host ULXs.
[i] The net ULXs per host galaxy.
[j] The net ULXs per survey galaxy.

population extracted from this survey by calculating the percentages of survey galaxies that host ULXs, the ULX rates per galaxy, the ULX rates per unit of stellar light, and the luminosity function. The calculations are carried out for ULXs above different luminosities to study the evolution with luminosity.

Some basic quantities are calculated for a survey of galaxies. For a luminosity bin (L_1, L_2), we calculate the observed number of ULXs $U_g(L_1, L_2)$ in each galaxy and the observed total number of ULXs $U(L_1, L_2)$ in all galaxies, the predicted number of contaminating sources $N_b^g(L_1, L_2)$ for each galaxy and the total number $N_b(L_1, L_2)$ for all galaxies, the surveyed blue light curve $\mathcal{L}_g(L)$ for each galaxy and the total surveyed blue light curve $\mathcal{L}(L)$ for all galaxies. The net number of ULXs for a survey in a luminosity bin (L_1, L_2) is calculated[1] as $N_t(L_1, L_2) = U(L_1, L_2) - N_b(L_1, L_2)$, with the nominal 1 σ error as the maximum of $[U(L_1, L_2)]^{1/2}$ and unity. The corresponding cumulative quantities, the observed cumulative number of ULXs $U(>L_1)$, the cumulative number of contaminating sources $N_b(>L_1)$, the cumulative net number of ULXs $N_t(>L_1)$ and its error, are calculated with L_2 set to 10^{42} ergs s^{-1}.

[1] Calculated net number of ULXs and derived ULX rates can be negative, either because of large downward fluctuations in the number of detections or overestimate of the background owing to cosmic variance. In such cases, the number/rates should be interpreted as equivalent to zeros.

The occurrence frequency, defined as the percentage of survey galaxies that host ULXs with luminosities above L, is calculated by comparing the number of survey galaxies for which ULXs with luminosities above L can be detected and the number that host ULXs with luminosities above L. The former, $N_{SG}(>L)$, is defined as the number of galaxies for which at least 10% of the blue light $\mathcal{L}g$ have detection thresholds below L. The latter, $N_{HG}(>L)$, is defined as the number of galaxies for which $U_g(>L) - N_b^g(>L) > 0.95$ (i.e., a galaxy with one ULX candidate and <0.05 contaminating sources as false ULXs is considered as a host galaxy). With these two numbers, the occurrence frequency is calculated as the minimum of 100% and $N_{HG}(>L)/N_{SG}(>L)$, and the error is calculated by considering the error in $N_{HG}(>L)$.

The ULX rates per survey/host galaxy are calculated for ULXs with luminosities above L. The ULX rate per survey galaxy is calculated as $N_t^S(>L)/N_{SG}(>L)$ with $N_t^S(>L)$ as the net number of ULXs in these $N_{SG}(>L)$ survey galaxies. The error for $N_t^S(>L)$ is the maximum of unity and $\left[U^S(>L)\right]^{1/2}$, where $U^S(>L)$ is the observed number of ULXs in these survey galaxies. Similarly, the ULX rate per host galaxy is calculated as $N_t^H(>L)/N_{HG}(>L)$ with $N_t^H(>L)$ as the net number of ULXs in the $N_{HG}(>L)$ host galaxies. The error for $N_t^H(>L)$ is the maximum of unity and $\left[U^H(>L)\right]^{1/2}$with $U^H(>L)$ as the observed number of ULXs in these host galaxies.

TABLE 1—*Continued*

Sample[a] (1)	$L_X \geq 4.0 \times 10^{39}$ ergs s^{-1} [d]					$L_X \geq 10^{40}$ ergs s^{-1} [e]				
	N_{SG}[f]	N_{HG}[g]	N_{HG}/N_{SG}[h]	N_U/N_{SG}[i]	N_U/N_{SG}[j]	N_{SG}[f]	N_{HG}[g]	N_{HG}/N_{SG}[h]	N_U/N_{SG}[i]	N_U/N_{SG}[j]
All	226	20	8.8 ± 2	1.20 ± 0.25	0.10 ± 0.025	281	8	2.8 ± 1	0.99 ± 0.35	0.023 ± 0.01
Early	67	3	4.5 ± 2.6	1.40 ± 0.73	0.05 ± 0.04	88	2	2.3 ± 1.6	1 ± 0.70	0.01 ± 0.016
Earlyx	65	2	3.1 ± 2.2	1.40 ± 0.85	0.03 ± 0.034	86	2	2.3 ± 1.6	1 ± 0.70	0.012 ± 0.016
Late	159	17	11 ± 2.6	1.16 ± 0.27	0.12 ± 0.03	193	6	3.1 ± 1.3	0.98 ± 0.40	0.03 ± 0.013
Pec	4	0	0 ± 0	0 ± 0	−0.025 ± 0.25	4	0	0 ± 0	0 ± 0	−0 ± 0.25
Ellip	34	1	2.9 ± 2.9	1.80 ± 1.40	0.05 ± 0.06	37	1	2.7 ± 2.7	1 ± 1	0.008 ± 0.027
Lent	33	2	6.1 ± 4.3	1.20 ± 0.85	0.06 ± 0.05	51	1	2 ± 2	1 ± 1	0.012 ± 0.02
Lentx	31	1	3.2 ± 3.2	1 ± 1	0.016 ± 0.03	49	1	2 ± 2	1 ± 1	0.016 ± 0.02
Sa	34	1	2.9 ± 2.9	1 ± 1	−0.012 ± 0.03	44	0	0 ± 0	0 ± 0	0.01 ± 0.023
Sb	63	6	9.5 ± 3.9	1.15 ± 0.43	0.12 ± 0.05	73	3	4.1 ± 2.4	1 ± 0.57	0.03 ± 0.023
Sc	60	9	15 ± 5	1.20 ± 0.37	0.15 ± 0.06	73	3	4.1 ± 2.4	0.97 ± 0.57	0.03 ± 0.023
Sd	32	4	12 ± 6.2	1 ± 0.50	0.15 ± 0.07	36	0	0 ± 0	0 ± 0	−0.003 ± 0.03
Sm	30	4	13 ± 6.7	1.25 ± 0.55	0.16 ± 0.07	32	1	3.1 ± 3.1	1 ± 1	0.03 ± 0.03
Sbrst	40	10	25 ± 7.9	1.19 ± 0.35	0.26 ± 0.08	46	2	4.3 ± 3.1	1 ± 0.70	0.06 ± 0.04
nSbrstL	123	7	5.7 ± 2.2	1.11 ± 0.40	0.07 ± 0.03	152	4	2.6 ± 1.3	0.97 ± 0.50	0.018 ± 0.013
SFRU	31	1	3.2 ± 3.2	2 ± 1.40	0.06 ± 0.045	41	0	0 ± 0	0 ± 0	−0.002 ± 0.024
SFRA	25	4	16 ± 8	1 ± 0.50	0.16 ± 0.08	26	1	3.8 ± 3.8	1 ± 1	0.04 ± 0.04
SFRB	27	4	15 ± 7.4	1 ± 0.50	0.14 ± 0.07	31	1	3.2 ± 3.2	1 ± 1	0.03 ± 0.03
SFRC	35	4	11 ± 5.7	1 ± 0.50	0.12 ± 0.06	47	0	0 ± 0	0 ± 0	−0.006 ± 0.02
SFRD	50	6	12 ± 4.9	0.98 ± 0.40	0.09 ± 0.05	65	1	1.5 ± 1.5	1 ± 1	0.009 ± 0.015
SFRE	33	3	9.1 ± 5.2	0.97 ± 0.57	0.09 ± 0.06	38	2	5.3 ± 3.7	1 ± 0.70	0.045 ± 0.04
SFRF	37	3	8.1 ± 4.7	0.97 ± 0.57	0.12 ± 0.07	41	1	2.4 ± 2.4	1 ± 1	0.012 ± 0.024
SFRG	40	5	12 ± 5.6	1.36 ± 0.52	0.18 ± 0.07	46	3	6.5 ± 3.8	0.97 ± 0.57	0.07 ± 0.04
SFRH	16	3	19 ± 11	1.63 ± 0.73	0.31 ± 0.15	19	3	16 ± 9.1	0.97 ± 0.57	0.19 ± 0.10

The ULX rate is also calculated as the number of ULXs per unit of blue stellar light to account for the variable sizes of survey galaxies. For a bin (L_1, L_2), the rate is calculated as

$$R(L_1, L_2) = \sum_{L_1 \leq L_i \leq L_2} \frac{1}{\mathcal{L}(L_i)} - \int_{L_1}^{L_2} \frac{dN_b(L, L + dL)}{\mathcal{L}(L)}.$$

Here the sum is over all observed ULXs in the bin, and gives the observed ULX rate; the integral gives the contamination rate, with $dN_b(L, L + dL)$ as the number of contaminating sources in the luminosity interval $(L, L + dL)$. The error $E(L_1, L_2)$ is computed as

$$E^2(L_1, L_2) = \sum_{L_1 \leq L_i \leq L_2} \frac{1}{\mathcal{L}^2(L_i)}.$$

If there are no observed ULXs in the bin, the error is defined as $E(L_1, L_2) = 1/\bar{\mathcal{L}}(L_1, L_2)$ with $\bar{\mathcal{L}}(L_1, L_2) = \int_{L_1}^{L_2} \mathcal{L}(L) d\log L / \int_{L_1}^{L_2} d\log L$ as the average of $\mathcal{L}(L)$ in the $\log L$ space. If the survey light curve is a constant of $\mathcal{L}$ in the bin, the above degenerates to $R(L_1, L_2) = [U(L_1, L_2) - N_b(L_1, L_2)]/\mathcal{L}$ and $E(L_1, L_2) = [U(L_1, L_2)]^{1/2}/\mathcal{L}$. For a bin (L_1, L_2), the cumulative ULX rate $R(>L_1)$ and its error $E(>L_1)$ are computed using the above expressions with L_2 set to 10^{42} ergs s^{-1}.

The above quantities are calculated for $L = 10^{38}$–10^{41} ergs s^{-1} in steps of $\Delta \log L = 0.2$. The quantities for some luminosities are tabulated to illustrate how they evolve with luminosity. In Table 1 the occurrence frequencies and ULX rates per galaxy are listed for ULXs above $\log L > 39$, 39.2, 39.6, and 40 in different surveys in our study. For each luminosity, we list (1) the number of survey galaxies, (2) the number of host galaxies, (3) the percentage, (4) the net number of ULXs per host galaxy, and (5) the net number of ULXs per survey galaxy. The ULX rates per unit of stellar light for different surveys are listed in Table 2 for bins $\log L = [39, 39.2]$ and $\log L = [39.2, 39.4]$, and in Table 3 for bins $\log L = [39.6, 39.8]$ and $\log L = [40, 40.2]$. For each bin, we list (1) the observed number and the observed cumulative number of ULXs, (2) the number and the cumulative number of contaminating sources, (3) the net number of ULXs and its error, (4) the cumulative net number of ULXs and its error, (5) the average blue light in the bin, (6) the ULX rate and its error, and (7) the cumulative ULX rate and its error.

The luminosity function of X-ray point sources is calculated as the ULX rate per unit of stellar light as a function of luminosity in the luminosity range from 10^{38} to 10^{41}. Such a luminosity range covers ULXs and the luminous end for high-mass X-ray binaries (HMXBs) and low-mass X-ray binaries (LMXBs) commonly seen in our Galaxy and nearby galaxies, and enables direct comparisons between ULXs and HMXB/LMXBs. The luminosity function is fitted to a power-law form of $dn/dL = \alpha L^{-\beta}$ with the maximum likelihood method. Since the source count $U_i = U(L_i, L_{i+1})$ in a bin $\log L = [L_i, L_{i+1}]$ follows a Poisson distribution with a mean $\mu_i = N_b(L_i, L_{i+1}) + N_p(\alpha, \beta; L_i, L_{i+1})$, the likelihood function $P(\alpha, \beta) = \Pi_i(\mu_i^{U_i}/U_i!)e^{-\mu_i}$. Here $N_b(L_i, L_{i+1})$ is the predicted contaminating sources in this bin, and $N_p(\alpha, \beta; L_i, L_{i+1}) = \int_{L_i}^{L_{i+1}} \alpha L^{-\beta} \mathcal{L}(L)\, dL$ is the number of sources predicted by the power-law model. In practice, $M \equiv -\ln P(\alpha, \beta)$ is minimized to obtain the best-fit values α_0 and β_0. Because $2\Delta M \equiv 2[M(\alpha_0 + \Delta\alpha, \beta_0 + \Delta\beta) - M(\alpha, \beta)]$ follows the χ^2 distribution of two degrees of freedom, the 68.3% (1 σ) confidence region on α and β jointly is demarcated by the contour of $2\Delta M = 2.3$, and the 68.3% confidence interval on α (β) is the projection of this region on the α (β) axis. The 95.4% (2 σ) confidence region corresponds to $2\Delta M = 6.2$, and 99.7% (3 σ) corresponds to $2\Delta M = 11.8$. The best fits are computed for ULX populations in some groups of galaxies and listed in Table 4.

3. PROPERTIES OF DIFFERENT ULX SAMPLES

3.1. *ULXs in All Galaxies*

The total HRI survey includes 313 galaxies, about 7.1% of the RC3 galaxies within 40 Mpc. Compared to the RC3 galaxies, the

TABLE 2

ULX Rates for Different Survey Galaxy Samples

			$\log L_X$ = [39, 39.2]							$\log L_X$ = [39.2,39.4]						
Sample[a]	NG[b]	LG[c]	ULX[d]	BG[e]	Net[f]	CNet[g]	SL/SFR[h]	Urate[i]	Crate[j]	ULX[d]	BG[e]	Net[f]	CNet[g]	SL/SFR[h]	Urate[i]	Crate[j]
All	296	0.78	22/89	5.7/26	16.3 ± 4.7	63 ± 9.4	59/95	0.26 ± 0.08	0.59 ± 0.10	14/67	5.9/20.3	8.1 ± 3.7	46.7 ± 8.2	91/130	0.1 ± 0.045	0.33 ± 0.06
Early	91	0.9	1/10	1.4/10.3	−0.4 ± 1	−0.3 ± 3.2	9.5/2.2	−0.079 ± 0.07	−0.13 ± 0.09	1/9	2.5/8.9	−1.5 ± 1	0.1 ± 3	28/3.6	−0.062 ± 0.026	−0.047 ± 0.05
Earlyx	89	0.8	1/7	1.4/8.8	−0.4 ± 1	−1.8 ± 2.6	8.0/0.5	−0.1 ± 0.08	−0.19 ± 0.09	0/6	2.2/7.4	−2.2 ± 1	−1.4 ± 2.4	23/1.3	−0.092 ± 0.04	−0.087 ± 0.05
Late	205	0.74	21/79	4.3/15.7	16.7 ± 4.6	63.3 ± 8.9	49/93	0.33 ± 0.09	0.84 ± 0.13	13/58	3.4/11.4	9.6 ± 3.6	46.6 ± 7.6	63/120	0.17 ± 0.06	0.51 ± 0.09
pec	5	0.52	0/0	0/0.1	−0 ± 1	−0.1 ± 1	1.3/15	−0.03 ± 0.75	−0.076 ± 0.39	0/0	0/0.1	−0 ± 1	−0.1 ± 1	1.3/15	−0.014 ± 0.75	−0.046 ± 0.39
Ellip	38	1.4	0/4	1.1/7.2	−1.1 ± 1	−3.2 ± 2	5.5/0.1	−0.22 ± 0.25	−0.34 ± 0.04	0/4	1.9/6.1	−1.9 ± 1	−2.1 ± 2	20/0.4	−0.094 ± 0.04	−0.12 ± 0.04
Lent	53	0.52	1/6	0.3/3.1	0.7 ± 1	2.9 ± 2.4	4.4/2.1	0.1 ± 0.17	0.19 ± 0.21	1/5	0.6/2.8	0.4 ± 1	2.2 ± 2.2	8.8/3.2	0.000 ± 0.07	0.09 ± 0.12
Lentx	51	0.33	1/3	0.3/1.6	0.7 ± 1	1.4 ± 1.7	2.9/0.4	0.13 ± 0.24	0.23 ± 0.33	0/2	0.3/1.3	−0.3 ± 1	0.7 ± 1.4	4.3/0.9	−0.073 ± 0.24	0.10 ± 0.22
Sa	45	0.8	2/9	1/4.8	1 ± 1.4	4.2 ± 3	10/4.4	0.10 ± 0.13	0.28 ± 0.19	3/7	1.1/3.8	1.9 ± 1.7	3.2 ± 2.6	16/18	0.15 ± 0.12	0.19 ± 0.14
Sb	77	1.2	9/35	2.7/9.8	6.3 ± 3	25.2 ± 5.9	27/50	0.22 ± 0.1	0.56 ± 0.14	6/26	2/7.1	4 ± 2.4	18.9 ± 5.1	35/68	0.12 ± 0.07	0.34 ± 0.10
Sc	75	0.94	13/43	2.3/7.1	10.7 ± 3.6	35.9 ± 6.6	24/36	0.42 ± 0.14	1 ± 0.2	5/30	1.6/4.7	3.4 ± 2.2	25.3 ± 5.5	30/53	0.12 ± 0.08	0.59 ± 0.13
Sd	40	0.35	8/20	0.9/2.1	7.1 ± 2.8	17.9 ± 4.5	8.9/18	0.78 ± 0.32	1.8 ± 0.45	2/12	0.5/1.2	1.5 ± 1.4	10.8 ± 3.5	9.9/18	0.15 ± 0.14	1 ± 0.33
Sm	36	0.077	2/9	0.1/0.4	1.9 ± 1.4	8.6 ± 3	1.2/0.4	1.4 ± 1.1	4.8 ± 1.8	2/7	0.1/0.3	1.9 ± 1.4	6.7 ± 2.6	1.4/0.5	1.4 ± 1	3.4 ± 1.4
Sbrst	46	0.66	13/35	1.1/3.1	11.9 ± 3.6	31.9 ± 5.9	17/45	0.69 ± 0.21	1.5 ± 0.29	2/22	0.8/2	1.2 ± 1.4	20 ± 4.7	19/48	0.06 ± 0.07	0.83 ± 0.2
nSbrstL	164	0.75	8/44	3.3/13.1	4.7 ± 2.8	30.9 ± 6.6	32/48	0.14 ± 0.09	0.57 ± 0.13	11/36	2.7/9.8	8.3 ± 3.3	26.2 ± 6	44/77	0.21 ± 0.08	0.42 ± 0.1
SFRU	44	0.13	1/4	0.1/0.6	0.9 ± 1	3.4 ± 2	0.5/0.04	1.6 ± 1.7	3.2 ± 2.3	1/3	0.1/0.5	0.9 ± 1	2.5 ± 1.7	0.6/0.07	1.4 ± 1.5	1.6 ± 1.5
SFRA	28	0.16	0/7	0.3/0.8	−0.3 ± 1	6.2 ± 2.6	3.4/0.5	−0.099 ± 0.3	1.5 ± 0.64	1/7	0.2/0.4	0.8 ± 1	6.6 ± 2.6	3.8/0.6	0.22 ± 0.27	1.6 ± 0.64
SFRB	33	0.17	0/7	0.3/0.8	−0.3 ± 1	6.2 ± 2.6	3.7/0.7	−0.094 ± 0.28	1.4 ± 0.6	1/7	0.2/0.5	0.8 ± 1	6.5 ± 2.6	4.1/0.8	0.2 ± 0.25	1.5 ± 0.6
SFRC	51	0.57	4/17	0.7/2.8	3.3 ± 2	14.2 ± 4.1	10/3.9	0.32 ± 0.2	1.1 ± 0.32	5/13	0.5/2.1	4.5 ± 2.2	10.9 ± 3.6	11/3.9	0.4 ± 0.2	0.76 ± 0.25
SFRD	71	0.63	4/19	1/4.3	3 ± 2	14.7 ± 4.4	13/6.7	0.22 ± 0.15	0.69 ± 0.22	5/15	0.9/3.3	4.1 ± 2.2	11.7 ± 3.9	18/9.4	0.24 ± 0.13	0.47 ± 0.16
SFRE	40	0.99	8/21	1.2/4.9	6.8 ± 2.8	16.1 ± 4.6	12/16	0.55 ± 0.23	0.9 ± 0.27	3/13	1.2/3.7	1.8 ± 1.7	9.3 ± 3.6	19/22	0.12 ± 0.11	0.35 ± 0.14
SFRF	42	1.5	16/40	2.6/7.3	13.4 ± 4	32.7 ± 6.3	26/42	0.5 ± 0.15	0.98 ± 0.2	5/24	1.8/4.8	3.2 ± 2.2	19.2 ± 4.9	31/55	0.11 ± 0.07	0.49 ± 0.13
SFRG	47	1.6	10/36	2/6.9	8 ± 3.2	29.1 ± 6	24/78	0.3 ± 0.12	0.77 ± 0.17	4/26	1.4/4.9	2.6 ± 2	21.1 ± 5.1	29/100	0.10 ± 0.07	0.47 ± 0.12
SFRH	19	1.8	0/9	0.3/2.7	−0.3 ± 1	6.3 ± 3	5.9/48	−0.057 ± 0.18	0.25 ± 0.18	1/9	0.4/2.4	0.6 ± 1	6.6 ± 3	9.7/64	0.10 ± 0.14	0.3 ± 0.18

[a] The survey galaxy groups based on galaxy types, presence of starburst, and star formation rates (SFR). An "x" is suffixed when the two peculiar lenticulars, NGC 1316 and NGC 5128, are excluded from the early-type and lenticular galaxy groups.

[b] Number of galaxies in this sample.

[c] The average blue light per galaxy in units of $10^{10}\ L_{\odot}$.

[d] Number of extranuclear X-ray sources observed in this bin, and the cumulative number.

[e] Number of predicted background/foreground X-ray sources that would have luminosity in this bin, and the cumulative number.

[f] The net number of X-ray sources in this bin, with errors as $(N_{\rm ULX})^{1/2}$.

[g] The cumulative net number of X-ray sources with luminosity of this bin and larger.

[h] Surveyed blue light in units of $10^{10}\ L_{\odot}$ and the total star formation rates in $M_{\odot}\ {\rm yr}^{-1}$ for the luminosity in this bin.

[i] The ULX rate in units of ULX per $10^{10}\ L_{\odot}$ in this bin.

[j] The ULX rate (ULX per $10^{10}\ L_{\odot}$) for luminosities in this bin and larger.

TABLE 3

ULX Rates for Different Survey Galaxy Samples

			$\log L_X$ = [39.6, 39.8]							$\log L_X$ = [40, 40.2]						
Sample[a]	NG[b]	LG[c]	ULX[d]	BG[e]	Net[f]	CNet[g]	SL/SFR[h]	Urate[i]	Crate[j]	ULX[d]	BG[e]	Net[f]	CNet[g]	SL/SFR[h]	Urate[h]	Crate[j]
All	296	0.78	13/34	3.7/9	9.3 ± 3.6	25 ± 5.8	170/250	0.05 ± 0.02	0.13 ± 0.03	1/9	1.4/2.6	−0.4 ± 1	6.4 ± 3	219/290	−0.002 ± 0.004	0.03 ± 0.013
Early	91	0.9	2/7	1.7/3.9	0.3 ± 1.4	3.1 ± 2.6	60/6	0.005 ± 0.023	0.04 ± 0.04	0/2	0.6/1.1	−0.6 ± 1	0.9 ± 1.4	79/17	−0.008 ± 0.013	0.01 ± 0.017
Earlyx	89	0.8	1/5	1.3/3.4	−0.3 ± 1	1.6 ± 2.2	49/3.6	−0.008 ± 0.018	0.02 ± 0.035	0/2	0.5/1	−0.5 ± 1	1 ± 1.4	69/15	−0.008 ± 0.014	0.014 ± 0.02
Late	205	0.74	11/27	2.1/5	8.9 ± 3.3	22 ± 5.2	110/240	0.08 ± 0.03	0.17 ± 0.04	1/7	0.8/1.5	0.2 ± 1	5.5 ± 2.6	139/270	0.001 ± 0.007	0.04 ± 0.018
Pec	5	0.52	0/0	0/0.1	−0 ± 1	−0.1 ± 1	1.7/26	−0.007 ± 0.75	−0.026 ± 0.39	0/0	0/0	−0 ± 1	−0 ± 1	2.6/26	−0.005 ± 0.39	−0.009 ± 0.39
Ellip	38	1.4	1/4	1.1/2.7	−0.1 ± 1	1.3 ± 2	40/1.4	−0.005 ± 0.02	0.023 ± 0.04	0/1	0.4/0.8	−0.4 ± 1	0.2 ± 1	53/1.7	−0.008 ± 0.02	0.005 ± 0.02
Lent	53	0.52	1/3	0.6/1.3	0.4 ± 1	1.7 ± 1.7	19/4.5	0.024 ± 0.05	0.07 ± 0.08	0/1	0.2/0.4	−0.2 ± 1	0.6 ± 1	26/16	−0.007 ± 0.04	0.023 ± 0.04
Lentx	51	0.33	0/1	0.2/0.7	−0.2 ± 1	0.3 ± 1	9.2/2.2	−0.026 ± 0.1	0.004 ± 0.06	0/1	0.1/0.2	−0.1 ± 1	0.8 ± 1	15/13	−0.008 ± 0.06	0.045 ± 0.06
Sa	45	0.8	1/2	0.7/1.6	0.3 ± 1	0.4 ± 1.4	28/56	0.007 ± 0.03	0.008 ± 0.04	0/1	0.3/0.5	−0.3 ± 1	0.5 ± 1	35/68	−0.007 ± 0.03	0.015 ± 0.03
Sb	77	1.2	5/11	1.3/3.1	3.7 ± 2.2	7.9 ± 3.3	69/150	0.05 ± 0.03	0.1 ± 0.04	0/3	0.5/0.9	−0.5 ± 1	2.1 ± 1.7	84/160	−0.005 ± 0.012	0.023 ± 0.02
Sc	75	0.94	7/13	0.8/2	6.2 ± 2.6	11 ± 3.6	49/87	0.13 ± 0.05	0.2 ± 0.07	1/3	0.3/0.6	0.7 ± 1	2.4 ± 1.7	65/110	0.01 ± 0.014	0.034 ± 0.025
Sd	40	0.35	3/5	0.2/0.4	2.8 ± 1.7	4.6 ± 2.2	11/19	0.24 ± 0.15	0.39 ± 0.19	0/0	0/0.1	−0 ± 1	−0.1 ± 1	12/20	−0.004 ± 0.08	−0.008 ± 0.07
Sm	36	0.077	1/5	0.1/0.1	0.9 ± 1	4.9 ± 2.2	2.3/0.7	0.42 ± 0.45	2 ± 0.93	0/1	0/0	−0 ± 1	1 ± 1	2.5/0.8	−0.006 ± 0.41	0.38 ± 0.4
Sbrst	46	0.66	5/13	0.3/0.8	4.7 ± 2.2	12.2 ± 3.6	23/72	0.2 ± 0.09	0.45 ± 0.13	0/3	0.2/0.3	−0.2 ± 1	2.7 ± 1.7	30/92	−0.005 ± 0.03	0.09 ± 0.06
nSbrstL	164	0.75	6/14	1.9/4.4	4.1 ± 2.4	9.6 ± 3.7	89/170	0.05 ± 0.03	0.10 ± 0.04	1/4	0.6/1.3	0.4 ± 1	2.7 ± 2	112/190	0.003 ± 0.009	0.023 ± 0.017
SFRU	44	0.13	0/2	0.1/0.4	−0.1 ± 1	1.6 ± 1.4	3.8/0.3	−0.036 ± 0.27	0.3 ± 0.27	0/0	0.1/0.1	−0.1 ± 1	−0.1 ± 1	5.5/0.4	−0.012 ± 0.18	−0.022 ± 0.17
SFRA	28	0.16	2/4	0.1/0.1	1.9 ± 1.4	3.9 ± 2	4.2/0.9	0.47 ± 0.34	0.9 ± 0.46	0/1	0/0	−0 ± 1	1 ± 1	4.5/1.0	−0.003 ± 0.22	0.22 ± 0.22
SFRB	33	0.17	2/4	0.1/0.1	1.9 ± 1.4	3.9 ± 2	4.4/1.1	0.44 ± 0.32	0.82 ± 0.43	0/1	0/0.1	−0 ± 1	0.9 ± 1	5.4/1.5	−0.005 ± 0.19	0.17 ± 0.18
SFRC	51	0.57	3/5	0.4/1.1	2.6 ± 1.7	3.9 ± 2.2	18/8	0.14 ± 0.09	0.19 ± 0.11	0/0	0.2/0.4	−0.2 ± 1	−0.4 ± 1	27/10	−0.007 ± 0.04	−0.013 ± 0.034
SFRD	71	0.63	3/7	0.6/1.6	2.4 ± 1.7	5.4 ± 2.6	31/20	0.07 ± 0.05	0.15 ± 0.07	0/1	0.2/0.5	−0.2 ± 1	0.5 ± 1	41/25	−0.006 ± 0.024	0.012 ± 0.02
SFRE	40	0.99	1/5	0.7/1.4	0.3 ± 1	3.6 ± 2.2	33/35	0.01 ± 0.03	0.10 ± 0.06	0/2	0.2/0.3	−0.2 ± 1	1.7 ± 1.4	38/40	−0.005 ± 0.026	0.04 ± 0.036
SFRF	42	1.5	2/6	0.8/1.7	1.2 ± 1.4	4.3 ± 2.4	47/79	0.026 ± 0.03	0.08 ± 0.05	0/1	0.3/0.5	−0.3 ± 1	0.5 ± 1	54/89	−0.005 ± 0.02	0.009 ± 0.018
SFRG	47	1.6	5/11	0.9/2.2	4.1 ± 2.2	8.8 ± 3.3	53/200	0.08 ± 0.04	0.15 ± 0.06	1/4	0.3/0.7	0.7 ± 1	3.3 ± 2	66/230	0.01 ± 0.015	0.05 ± 0.03
SFRH	19	1.8	4/8	0.5/1.2	3.5 ± 2	6.8 ± 2.8	24/140	0.15 ± 0.08	0.24 ± 0.1	1/4	0.2/0.4	0.8 ± 1	3.6 ± 2	33/160	0.024 ± 0.03	0.11 ± 0.06

[a] The survey galaxy groups based on galaxy types, presence of starburst, and star formation rates (SFR). An "x" is suffixed when the two peculiar lenticulars, NGC 1316 and NGC 5128, are excluded from the early-type and lenticular galaxy groups.

[b] Number of galaxies in this sample.

[c] The average blue light per galaxy in units of $10^{10}\ L_{\odot}$.

[d] Number of extranuclear X-ray sources observed in this bin, and the cumulative number.

[e] Number of predicted background/foreground X-ray sources that would have luminosity in this bin, and the cumulative number.

[f] The net number of X-ray sources in this bin, with errors as $(N_{\mathrm{ULX}\cdot})^{1/2}$

[g] The cumulative net number of X-ray sources with luminosity of this bin and larger.

[h] Surveyed blue light in units of $10^{10}\ L_{\odot}$ and the total star formation rate in $M_{\odot}\ \mathrm{yr}^{-1}$ for the luminosity in this bin.

[i] The ULX rate in units of ULX per $10^{10}\ L_{\odot}$ in this bin.

[j] The ULX rate (ULX per $10^{10}\ L_{\odot}$) for luminosities in this bin and larger.

TABLE 4
Power-Law Fits to Luminosity Functions

Galaxies	$\log L_1 - \log L_2$[a]	α_0	$\pm\sigma$[b]	$\pm 2\ \sigma$	$\pm 3\ \sigma$	β_0	$\pm\sigma$	$\pm 2\ \sigma$	$\pm 3\ \sigma$
All	38.4–40	0.57	+0.15–0.14	+0.26–0.22	+0.36–0.29	1.93	+0.24–0.24	+0.40–0.40	+0.56–0.56
Late.....	38.4–40	0.65	+0.17–0.16	+0.29–0.25	+0.41–0.33	1.74	+0.22–0.23	+0.37–0.38	+0.52–0.54
Sbrst	38.4–40	1.14	+0.34–0.30	+0.59–0.46	+0.84–0.61	1.62	+0.28–0.27	+0.46–0.45	+0.65–0.63
nSbrstL.....	39–40	0.61	+0.47–0.31	+0.89–0.44	+1.39–0.53	2.00	+0.54–0.52	+0.93–0.89	+1.38–1.13

[a] The luminosity interval in which the fit is carried out.
[b] The confidence intervals are on α_0 and β_0 jointly.

survey galaxies are slightly larger, closer, and optically or X-ray brighter. In spite of slight overabundances of ellipticals, lenticulars and S0/a–Sc early spirals, and an underabundance of dwarf spirals and irregulars, the survey galaxy sample is representative of the nearby galaxies by morphological types. The ULX sample extracted from these galaxies is thus expected to be representative of surveys without large biases in galaxy types, and its properties can be used as standards for comparison with the properties of ULX samples from different groups of galaxies.

A deep survey is constructed from observations of all galaxies with the contamination from background/foreground objects calculated following the procedures in § 2. This surveys a total sky of 1.65 deg^2 and a total blue light of $2.3 \times 10^{12}\ L_\odot$, with an average sensitivity of about 2×10^{-14} ergs s^{-1} cm^{-2} in flux and 4×10^{39} ergs s^{-1} in luminosity (Fig. 1). With the $\log N - \log S$ relation, 26 contaminating sources with apparent luminosities above 10^{39} ergs s^{-1} are predicted as false ULXs for the surveyed area within the isophotes of galaxies, about 29% of the 89 detected ULXs. The contamination rate is 30% (20.3/67) for ULXs above 1.6×10^{39} ergs s^{-1}, 26% (9/26) for ULXs above 4.0×10^{39} ergs s^{-1}, and 29% (2.6/9) for ULXs above 10^{40} ergs s^{-1}.

The occurrence frequencies and ULX rates are calculated with the procedures in § 2.4 and tabulated in Table 1–3. As shown by the calculation, there are 98 galaxies that could have a ULX above 10^{39} ergs s^{-1} detectable, and 35 galaxies (i.e., 36% of the 98 galaxies) host a net number of $\geq$0.95 ULXs. The occurrence frequency is 25% (33/131) for ULXs above 1.6×10^{39} ergs s^{-1}, 8.8% (20/226) for ULXs above 4.0×10^{39} ergs s^{-1}, and 3% (8/281) for ULXs above 10^{40} ergs s^{-1}. The ULX rates are 0.56 ± 0.08, 0.32 ± 0.06, 0.10 ± 0.02, and 0.02 ± 0.01 ULXs per survey galaxy and 0.59 ± 0.10, 0.33 ± 0.06, 0.13 ± 0.03, and 0.03 ± 0.01 ULXs per $10^{10}\ L_\odot$ for ULXs above (1, 1.6, 4, and 10) $\times$ 10^{39} ergs s^{-1}, respectively. Given the average of $\sim 0.8 \times 10^{10}\ L_\odot$ per survey galaxy, the ULX rates per $10^{10}\ M_\odot$ are consistent with the ULX rates per survey galaxy.

The average survey is computed for all galaxies in comparison to the deep survey. In the average survey, the occurrence frequency is 40% (34/84) for ULXs above 10^{39} ergs s^{-1}, 28% (32/113) for ULXs above 1.6×10^{39} ergs s^{-1}, 8.9% (19/212) for ULXs above 4×10^{39} ergs s^{-1}, and 3.8% (10/271) for ULXs above 10^{40} ergs s^{-1}. The ULX rates are 0.52 ± 0.09, 0.32 ± 0.08, 0.09 ± 0.02, and 0.03 ± 0.01 ULXs per survey galaxy, and 0.70 ± 0.12, 0.38 ± 0.07, 0.11 ± 0.03, and 0.04 ± 0.02 ULXs per $10^{10}\ L_\odot$ for ULXs above (1, 1.6, 4, and 10) $\times$ 10^{39} ergs s^{-1}, respectively. These occurrence frequencies and ULX rates are consistent with those in the deep survey; we will not list them for the surveys of galaxies in the following subsections.

The luminosity function of the X-ray point sources is calculated following the procedures in § 2.4. The histograms of detected sources and predicted contaminating sources are shown in Figure 2, and a sharp drop at 10^{40} ergs s^{-1} is apparent in the detected sources. Given the surveyed blue light curve (Fig. 1),

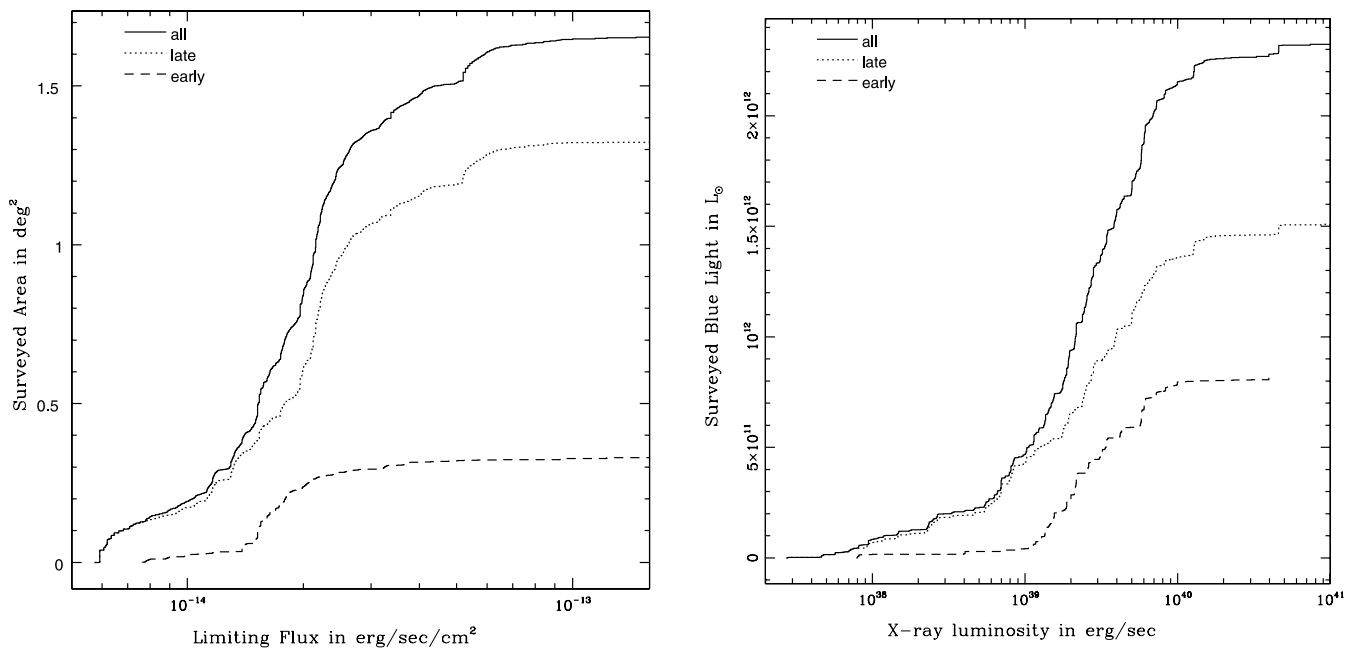

Fig. 1.—Surveyed area curve (*left*) and the surveyed blue light curve (*right*) for all galaxies (*solid line*), for late-type galaxies (*dotted line*) and for early-type galaxies (*dashed line*).

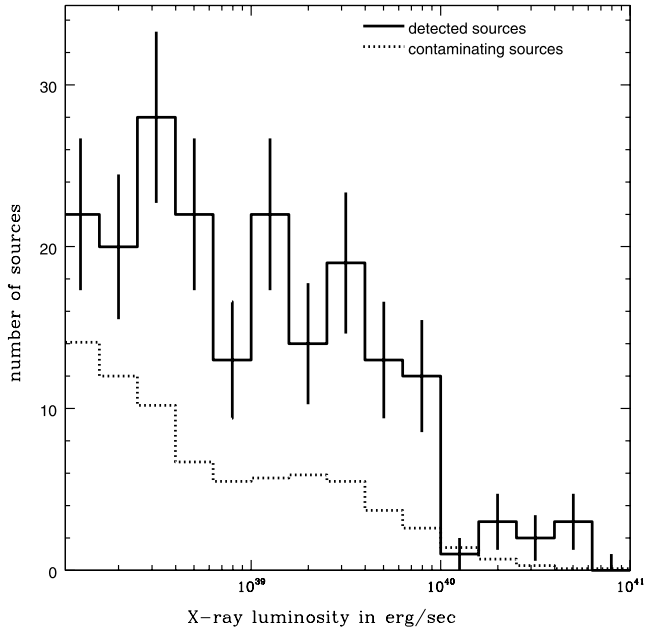

FIG. 2.—Detected nonnuclear sources and the contaminating sources from background/foreground in the survey of all galaxies.

the detected sources and the contaminating sources, the luminosity function can be fitted to a power law of $dn/dL = 0.57^{+0.15}_{-0.14}L^{-1.93^{+0.24}_{-0.24}}$ per $10^{10}\,L_{\odot}$ in the luminosity range of 2.5×10^{38}–10^{40} ergs s^{-1} (Table 4). The best fit and the confidence regions are shown in Figure 3 as contours of $2\Delta M$ as described in § 2.4. The luminosity function is plotted in Figure 4, with the best-fit power law and its errors overplotted for comparison. There are no changes of the slope or the normalization in the luminosity function around 10^{39} ergs s^{-1} between the ULX population and the lower luminosity HMXB/LMXB populations. Corresponding to the sharp drop in the detected sources (Fig. 2),

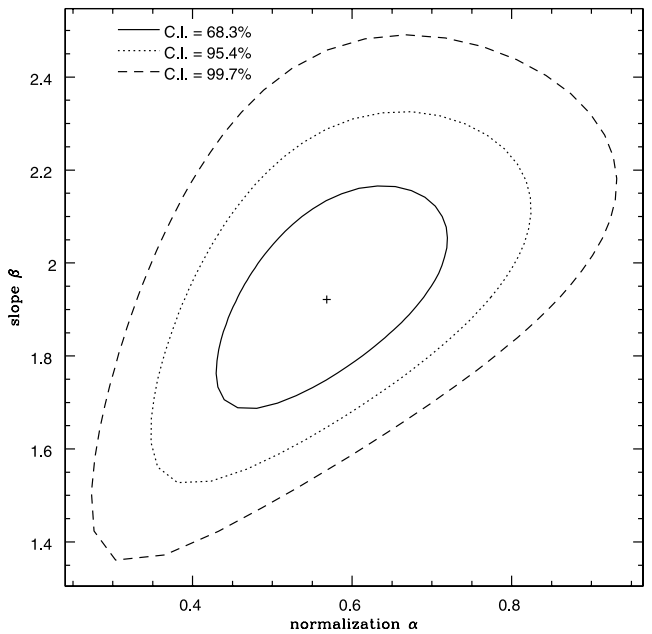

FIG. 3.—Power-law fit of the luminosity function for nonnuclear X-ray point sources in all galaxies. The best-fit parameters ($\alpha_0 = 0.57$, $\beta = 1.93$) are obtained by minimizing $M(\alpha, \beta)$. The 68.3% (1 σ), 95.4% (2 σ), and 99.7% (3 σ) confidence regions on α and β jointly are demarcated by the contours of $2\Delta M = 2.3$, 6.2, 11.8, respectively.

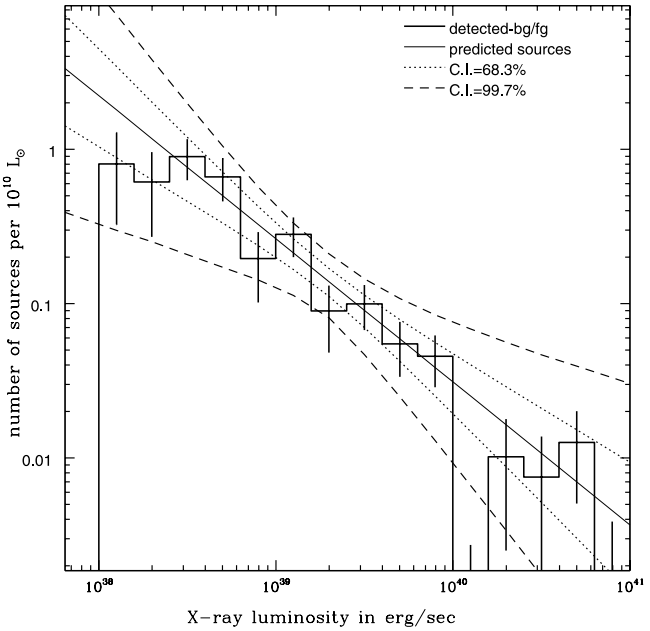

FIG. 4.—Luminosity function for the X-ray point sources in all galaxies. The histogram shows the number of detected sources (excluding the contaminating sources) per $10^{10}\,L_{\odot}$. The solid line is the prediction of the power-law fit to the luminosity function, and the dotted (dashed) lines enclose the uncertainty range allowed by the 1 (3) σ error in the best-fit parameters.

a gap is present at 10^{40} ergs s^{-1} in the luminosity function, with a deficit of ULXs more than accountable by the 3 σ error in the power-law fit. The luminosity function bends down at energies below 2×10^{38} ergs s^{-1} due to incompleteness.

3.2. *ULXs in Galaxies of Different Types*

In our analysis, the galaxies are divided into early-type galaxies, late-type galaxies, and peculiar galaxies, and further into subtypes as elliptical, lenticular, Sa, Sb, Sc, Sd, and Sm galaxies based on the Hubble type T (Table 5). The survey galaxies cover a complete range of morphological types and provide a chance to study the ULX populations in different types of galaxies with a uniform data set.

The contamination fraction of the ULX sample from the early-type galaxies is much higher than that from the late-type galaxies (Tables 2–3). In the deep survey of the early-type galaxies, 10 ULXs above 10^{39} ergs s^{-1} are detected, while 10.3 contaminating sources are predicted for its surveyed area of 0.33 square degrees. For the late-type galaxies, 79 ULXs above 10^{39} ergs s^{-1} are detected, while 15.7 contaminating sources are predicted for its surveyed area of 1.32 deg^2. The contamination fractions indicate that 63 (80%) of the ULXs from the late-type galaxies are true ULXs, and the ULX sample from the early-type galaxies is dominated by contaminating sources.

A significant preference for ULXs to occur in the late-type galaxies is clearly shown in the statistical results of the occurrence frequencies and ULX rates (Tables 1–3). The occurrence frequency for ULXs above 10^{39} ergs s^{-1} is 45% ± 8% (34/76) in the late-type galaxies, at least 4 times higher than the 4.5% ± 4.5% (1/22) in the early-type galaxies. The ULX rate per survey galaxy for ULXs above 10^{39} ergs s^{-1} is 0.72 ± 0.11, at least 5 times higher than that in the early-type galaxies (0.02 ± 0.11). The preference is less significant for ULXs with higher luminosities, and becomes inconclusive within 1 σ errors for ULXs above 10^{40} ergs s^{-1} due to the small number of such ULXs detected in this survey.

TABLE 5
GROUPING GALAXIES BASED ON DIFFERENT PROPERTIES

Group	No. of Galaxies	Lower Limit	Upper Limit	Average
Group Galaxies Based on the Hubble Type T				
Early	91	−6	−1	...
Late	205	0	11	...
Peculiar	5	90	99	...
Elliptical	38	−6	−4	−5
Lenticular	53	−3	−1	−2
Sa	45	0	2	1
Sb	77	2	4	3
Sc	75	4	6	5
Sd	40	6	8	7
Sm	36	9	11	10
Group Late-Type Galaxies Based on Star Formation Rates ($M_\odot$ yr^{-1})				
SFRU[a]	44	...	...	<0.0098
SFRA	28	...	0.09	0.035
SFRB	33	...	0.1	0.045
SFRC	51	0.09	0.5	0.23
SFRD	71	0.1	1	0.39
SFRE	40	0.5	1.8	1.02
SFRF	42	1	4	2.18
SFRG	47	1.8	...	4.94
SFRH	19	4	...	8.51

[a] This group includes galaxies with only upper limits in the flux densities at 60 μm.

The luminosity functions are calculated for the X-ray sources in the early-type galaxies (Fig. 5) and in the late-type galaxies (Fig. 6). For the early-type galaxies, there are more X-ray sources per surveyed blue light below 10^{39} ergs s^{-1} than for the sample of all galaxies. The luminosity function shows a sharp cutoff around 10^{39} ergs s^{-1} since there are about equal numbers of detected sources and predicted contaminating sources above 10^{39} ergs s^{-1}. For the late-type galaxies, there is no similar cutoff around 10^{39} ergs s^{-1}, and the ULX population above 10^{39} ergs s^{-1} is a smooth extension of the LMXB/HMXB populations except for a gap at 10^{40} ergs s^{-1} in the luminosity function, as present in the luminosity function for X-ray sources in all galaxies (Fig. 4). The luminosity function can be fitted with a power-law of $dn/dL = 0.65^{+0.17}_{-0.16} L^{-1.74^{+0.22}_{-0.23}}$ per $10^{10}\,L_\odot$ in the luminosity range of 2.5×10^{38}–10^{40} ergs s^{-1}.

The statistical properties of ULX samples from different subtypes of galaxies are calculated (Tables 1–3) to reveal possible trends with galaxy subtypes. The occurrence frequencies and ULX rates generally increase with the Hubble type T until they peak at Sc, then decrease with T (Figs. 7–8). For Sc galaxies, the occurrence frequency (the ULX rate per survey galaxy) is 59% ± 14% (1.10 ± 0.21) for ULXs above 10^{39} ergs s^{-1}, higher than those for the average late-type galaxies and the early-type galaxies. When scaled by the surveyed blue light, the ULX rates increases monotonically with T, and the rates in Sm spirals are highest among the subtypes of galaxies due to the small sizes of Sm spirals ($0.077 \times 10^{10}\,L_\odot$ per Sm galaxy as compared to $0.94 \times 10^{10}\,L_\odot$ per Sc galaxy).

3.3. *ULXs in Starburst and Nonstarburst Galaxies*

Many ULXs have been found to reside in star-forming regions, which leads to the conclusion that ULXs are closely related to star formation activities. To test this connection, we group galaxies based on whether they are starburst galaxies that have significant *current* star formation activities. While no single definition of the starburst phenomenon exists, the survey galaxies listed as starburst or H II galaxies in NED are included in the starburst galaxy group (Sbrst), which include 46 out of 313 survey galaxies, with two E0 ellipticals, three dwarf lenticulars and 41 late-type galaxies. For comparison also constructed is another group of 164 nonstarburst late-type galaxies (nSbrstL). We caution that the list of starburst/H II galaxies is not complete, and some galaxies in the nonstarburst galaxy group may be starburst galaxies.

The contamination fraction of the ULX sample from the starburst galaxies is much lower than the fractions from nonstarburst

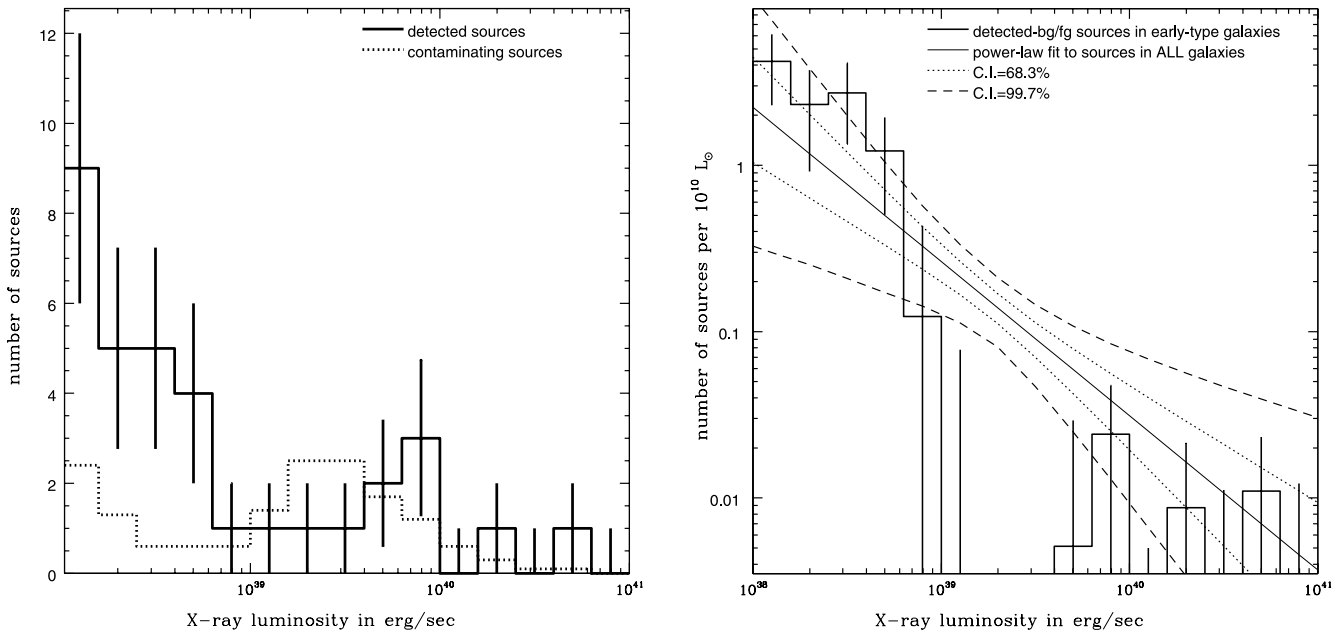

FIG. 5.—Histograms of the detected sources and the contaminating sources in early-type galaxies (*left*), and the luminosity function scaled by the surveyed blue light (*right*). The luminosity function shows a cutoff around 10^{39} ergs s^{-1}, and no power law is fitted to this function. The power-law fit and its errors for sources in all galaxies are overplotted for comparison.

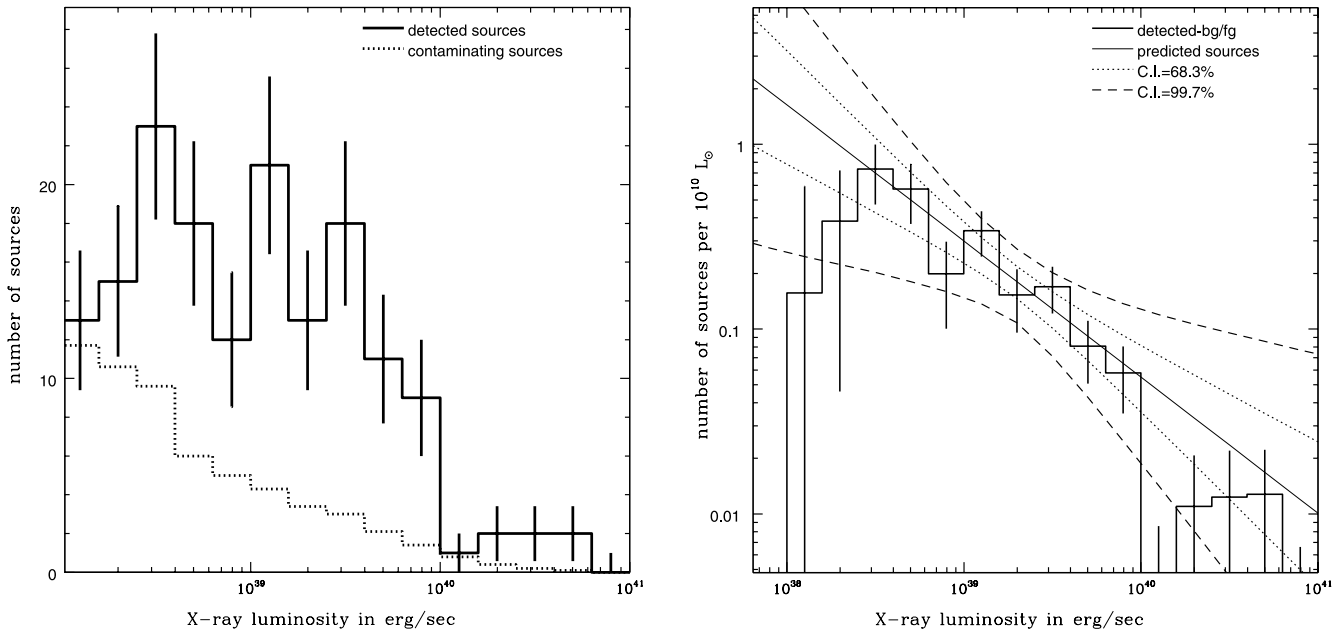

FIG. 6.—Histograms of the detected sources and the contaminating sources in late-type galaxies (*left*), and the luminosity function scaled by the surveyed blue light (*right*). The power-law fit to this luminosity function and its errors are overplotted for comparison.

galaxies. In the deep survey of the starburst galaxies, 3.1 contaminating sources are predicted, while 35 ULXs are detected above 10^{39} ergs s^{-1}. The contamination fraction (9%) is much lower than that for nonstarburst late-type galaxies (29%) or for early-type galaxies (100%). The lowest contamination fraction implies that the starburst galaxies have the highest ULX surface density as compared to the other groups of galaxies, given that the number of contaminating sources is determined by the surface areas of the galaxies.

The occurrence frequencies and ULX rates in the starburst galaxies are higher than those in other types of galaxies. For ULXs above 10^{39} ergs s^{-1}, the occurrence frequency in starburst galaxies is 69% ± 16% (18/26), much higher than that in the nonstarburst late-type galaxies (31% ± 8%) or in the early-type galaxies (4.5%± 4.5%). The ULX rates per survey galaxy in the starburst galaxies are 0.98 ± 0.20, about 2 times higher than the rates of 0.56 ± 0.12 in the nonstarburst late-type galaxies. The contrast becomes stronger in the ULX rate per $10^{10}\,L_{\odot}$, which is 1.5 ± 0.29 for the starburst galaxies and 0.57 ± 0.13 for the nonstarburst galaxies. For the extreme ULXs above 10^{40} ergs s^{-1},

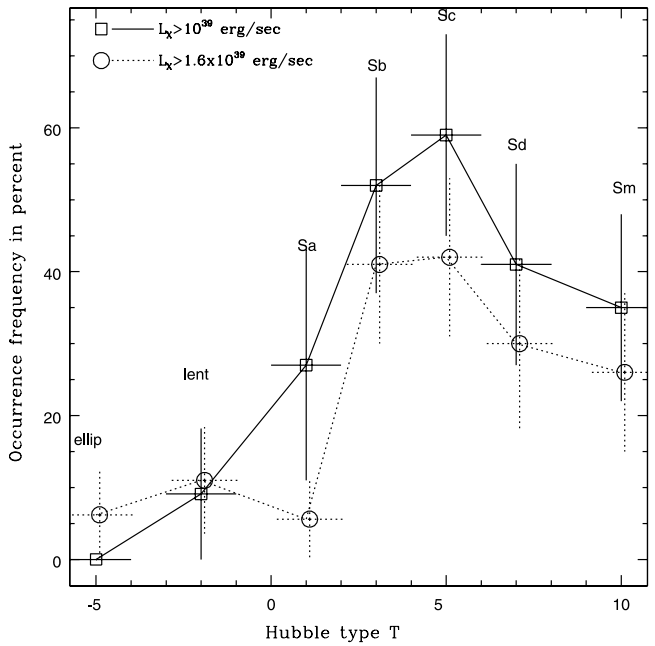

FIG. 7.—Occurrence frequencies of ULXs above 1×10^{39} and 1.6×10^{39} ergs s^{-1} in galaxies of different Hubble type T. The graph is based on the occurrence frequencies for subtypes of galaxies (Table 1), while the Hubble T for each subtype is listed in Table 5. The data points are offset slightly in the abscissa to separate the error bars.

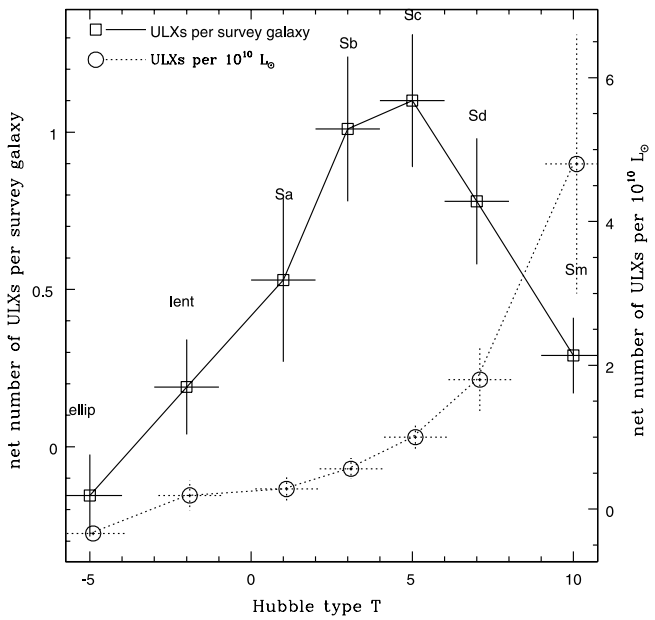

FIG. 8.—ULX rates per surveyed galaxy and per $10^{10}\,L_{\odot}$ as a function of the Hubble type T of survey galaxies for ULXs above 10^{39} ergs s^{-1}. The false ULXs due to background/foreground objects are removed from the detected ULXs in the calculation of the ULX rates (Table 1).

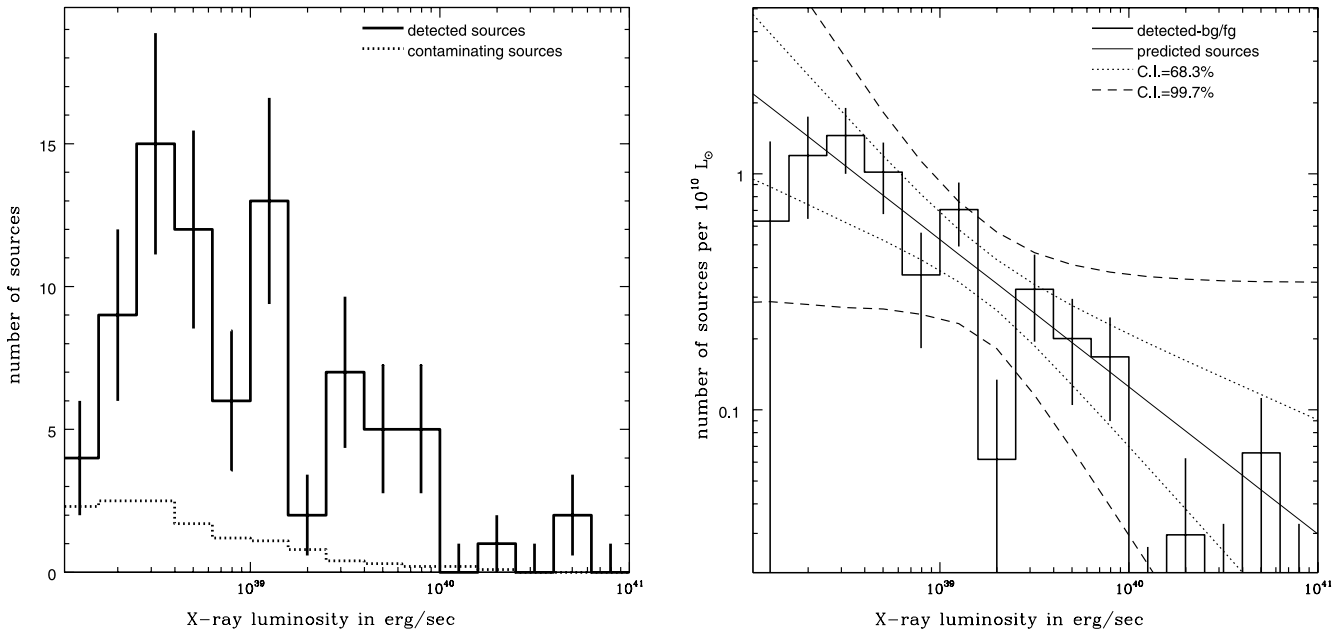

FIG. 9.—Histograms of the detected sources and the contaminating sources in starburst galaxies (*left*), and the luminosity function scaled by the surveyed blue light (*right*). The power-law fit to this luminosity function and its errors are overplotted for comparison.

the occurrence frequencies and ULX rates in the starburst galaxies may be higher than those in other types of galaxies, but given the small number statistics, they are consistent with being the same within 1 σ errors.

The luminosity functions are calculated for the X-ray sources in the starburst galaxies (Fig. 9) and in the nonstarburst late-type galaxies (Fig. 10). For the X-ray sources in the starburst galaxies, the luminosity function shows no significant breaks around 10^{39} ergs s^{-1}, and can be fitted with a power-law form of $dn/dL = 1.14^{+0.34}_{-0.30} L^{-1.62^{+0.28}_{-0.27}}$ per $10^{10}\,L_\odot$ in the luminosity range of 2.5×10^{38}–10^{40} ergs s^{-1}. For sources in the nonstarburst galaxies, the luminosity function begins to bend down around 10^{39} ergs s^{-1} due to incompleteness, and the part in the luminosity range of 10^{39}–10^{40} ergs s^{-1} can be fitted with a power law of $dn/dL = 0.61^{+0.47}_{-0.31}\ L^{-2.01^{+0.53}_{-0.52}}$ per $10^{10}\,L_\odot$.

3.4. *ULXs in Galaxies with Different Star Formation Rates*

To quantify the relation between star formation and the ULX phenomenon, we group the galaxies based on their star formation rates. The star formation rate is calculated with SFR($M_\odot$ yr^{-1}) = $4.5 \times 10^{-44}\ L(60\ \mu\mathrm{m})$ (Rosa-González et al. 2002). The flux densities at 60 μm, listed in Table 1 of Paper I (Liu & Bregman 2005), are taken from the *IRAS* Point Source Catalog (1986), with some nearby galaxies from Rice et al. (1988). For 102 galaxies that are not detected, the 3 σ upper limit is calculated by adopting noise levels of 8.5 mJy arcmin^{-2} (Rice et al. 1988).

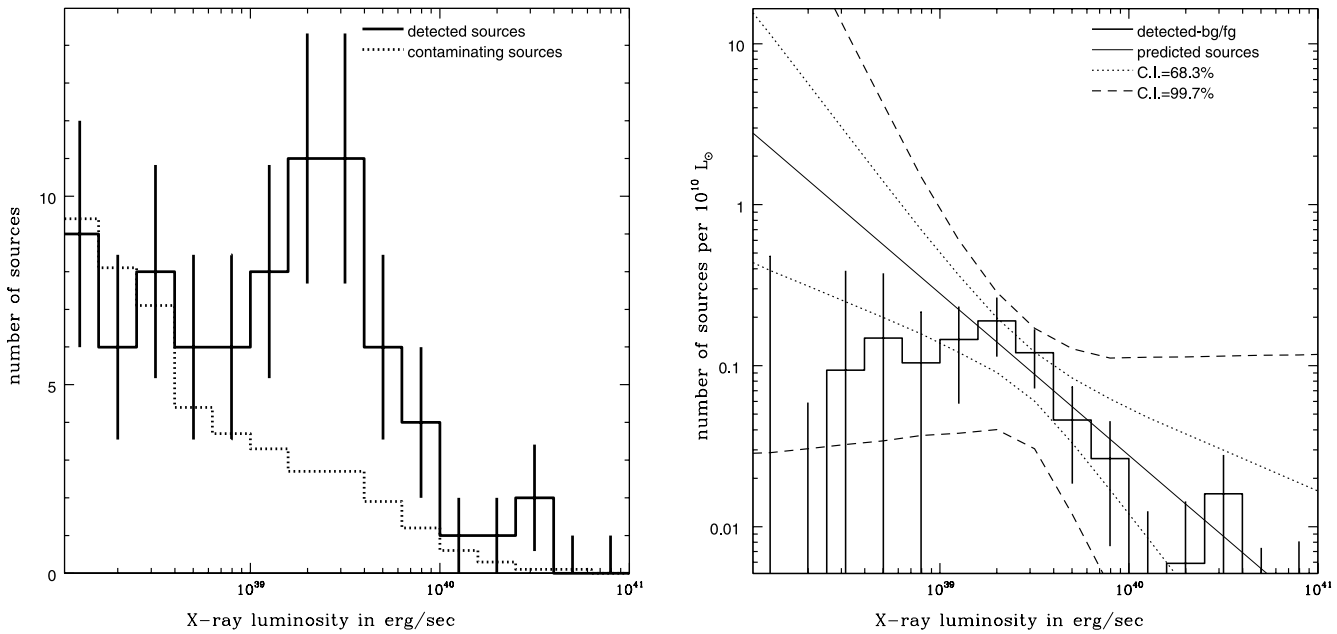

FIG. 10.—Histograms of the detected sources and the contaminating sources in nonstarburst late-type galaxies (*left*), and the luminosity function scaled by the surveyed blue light (*right*). The power-law fit to this luminosity function and its errors are overplotted for comparison.

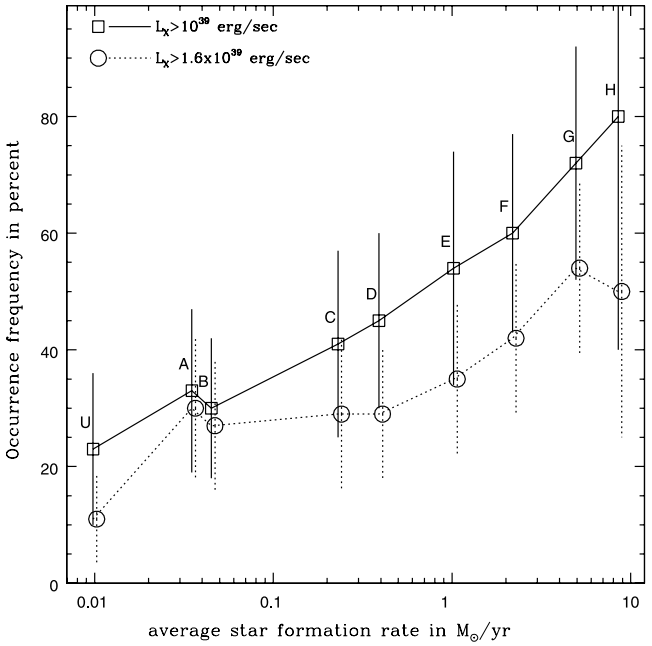

FIG. 11.—Occurrence frequencies of ULXs above 1×10^{39} and 1.6×10^{39} ergs s^{-1} in galaxies of different star formation rates. The occurrence frequencies for the SFR groups are taken from Table 1, with the average star formation rate for each group (labeled by name) taken from Table 5.

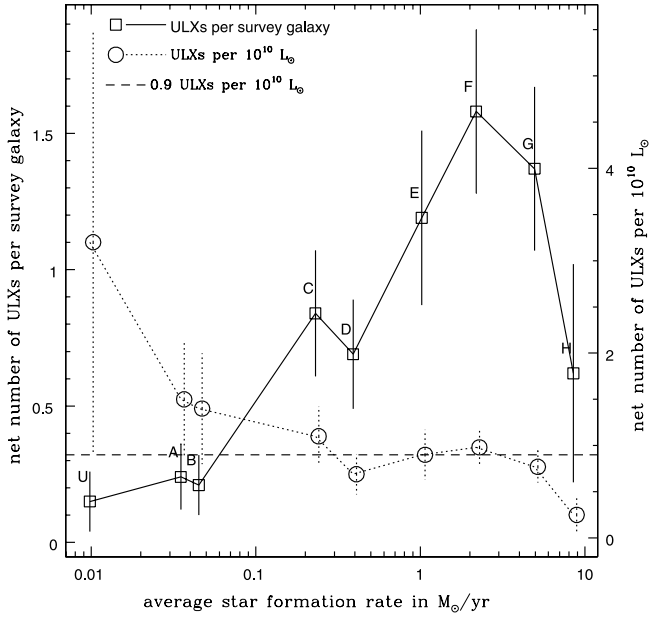

FIG. 12.—ULX rates per surveyed galaxy and per 10^{10} $L_\odot$ as a function of the star formation rates of galaxies for ULXs above 10^{39} ergs s^{-1}. The ULX rates per 10^{10} $L_\odot$ are consistent with a constant 0.9 ULXs per 10^{10} $L_\odot$ for galaxies with different star formation rates. The contaminating sources are removed in the calculation.

The calculated rates are compared to the compilation of Grimm et al. (2003) for 11 galaxies, and are consistent with their rates within 50% without systematic biases. Since the early-type galaxies are known to lack current star formation, we put only the late-type galaxies into nine SFR groups (SFRU and SFRA–SFRH) in the increasing order of star formation rates (Table 5).

The occurrence frequencies and ULX rates increase with the star formation rates of the galaxies (Tables 1–3). The occurrence frequency increases monotonically, from $12\% \pm 7\%$ for the group SFRU (<0.009 $M_\odot$ yr^{-1}) to $72\% \pm 20\%$ for the group SFRG (~ 5 $M_\odot$ yr^{-1}) for ULXs above 10^{39} ergs s^{-1} (Fig. 11). There is a general increase trend in the ULX rates per survey galaxy (Fig.12), from 0.03 ± 0.08 for the group SFRU to 1.55 ± 0.29 for the group SFRF (~ 2 $M_\odot$ yr^{-1}), albeit with large scatters and a possible drop for galaxies with ≥ 5 $M_\odot$ yr^{-1} (groups SFRG and SFRH). The ULX rates per 10^{10} $L_\odot$ show a decrease trend due to the increasing blue light contents for galaxies with larger star formation rates. The ULX rates, however, are consistent with a constant rate of 0.9 ULXs per 10^{10} $L_\odot$ within 1 σ errors except for the group SFRH.

The general increase of occurrence frequencies and ULX rates with the star formation rates suggests a linear relation between the two quantities. Grimm et al. (2003) tested the hypothesis with *Chandra* observations of 12 nearby starburst galaxies with SFR ≥ 1 $M_\odot$ yr^{-1} in which the HMXBs are assumed to dominate the X-ray sources, and found a universal luminosity function, i.e., $(dN/dL_{38}) = 3.3^{+1.1}_{-0.8}\mathrm{SFR}L_{38}^{-1.61\pm0.12}$ with a cutoff at $L_c = 2 \times 10^{40}$ ergs s^{-1}, where L_{38} is the X-ray luminosity in units of 10^{38} ergs s^{-1}, and SFR is in units of $M_\odot$ yr^{-1}. The number of X-ray sources above L_X expected from a galaxy can be obtained by integrating dN/dL over the luminosity range of L_X–L_c and is linearly proportional to the star formation rate of the host galaxy, i.e., $N_{\mathrm{ULX}} = \beta\mathrm{SFR}$. Note that the luminosity is calculated in 2–10 keV in Grimm et al. (2003), and is about 1.5 times lower than the luminosity in 0.3–8 keV for a power-law spectrum with $\Gamma = 1.7$ as adopted in this paper. Given this luminosity difference, $\beta = 0.85$, 0.25, and 0.05 for ULXs above 1, 4, and 10×10^{39} ergs s^{-1}, respectively.

This linear relation between the star formation rate and the expected number of ULXs can be tested with the HRI survey. The star formation rates of the survey galaxies span from <0.001 $M_\odot$ yr^{-1} to 15 $M_\odot$ yr^{-1} with a median of 0.1 $M_\odot$ yr^{-1}, and many ($\sim$80%) galaxies are expected to host less than one ULX. The star formation rates and the ULXs are summed for all galaxies in

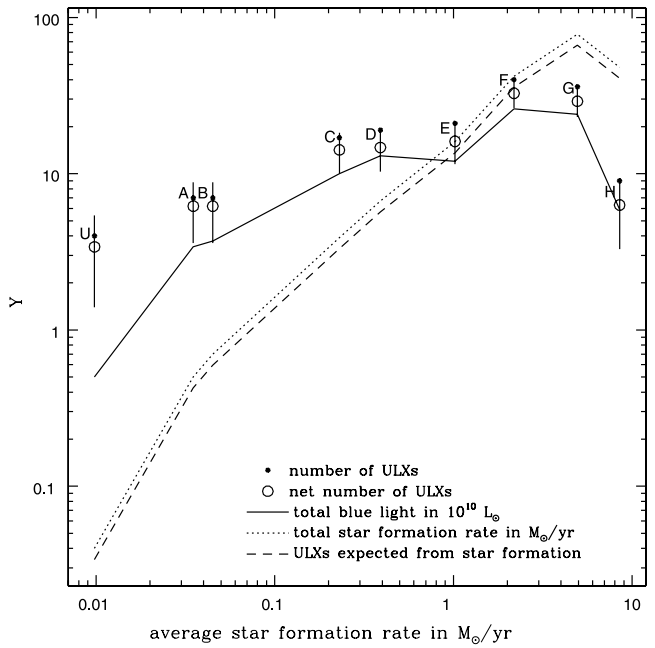

FIG. 13.—Detected ULX, the total star formation rates, and the total surveyed blue light for ULXs above 10^{39} ergs s^{-1} for the nine SFR groups with different star formation rates. The ULXs expected from star formation based on the N_{ULX}-SFR linear relation (Grimm et al. 2003) are plotted for comparison. The same *Y*-axis gives the scales for all the above quantities.

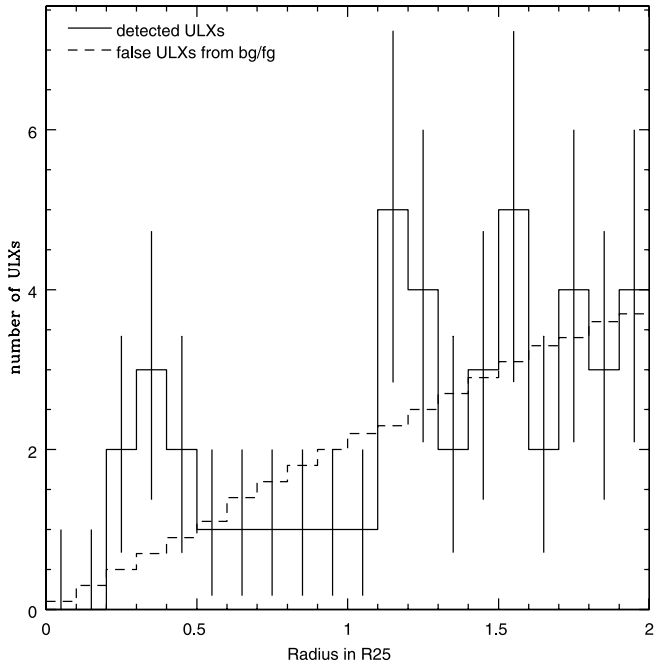

FIG. 14.—Radial distributions of detected ULXs and predicted contaminating sources above 10^{39} ergs s^{-1} in the early-type galaxies.

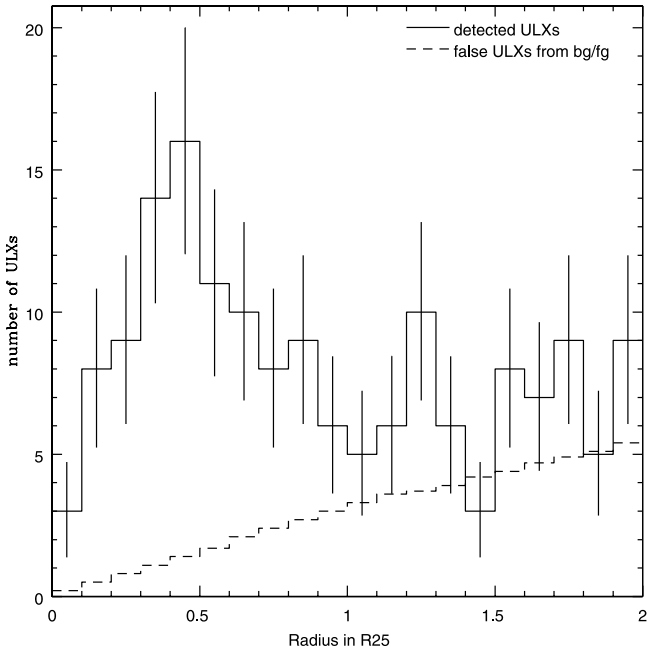

FIG. 15.—Radial distributions of detected ULXs and predicted contaminating sources above 10^{39} ergs s^{-1} in the late-type galaxies.

a group to reduce the statistical fluctuation caused by the small number of expected ULXs in individual galaxies. The detected ULXs above 10^{39} ergs s^{-1} are compared to the total surveyed blue light, the total star formation rates, and the ULXs expected from the star formation for the nine SFR groups (Fig. 13). The numbers of detected ULXs (with contaminating sources subtracted) are consistent with the numbers of expected ULXs for galaxies with $1\ M_\odot\ \mathrm{yr}^{-1} \leq \mathrm{SFR} \leq 3\ M_\odot\ \mathrm{yr}^{-1}$ in groups SFRE and SFRF. The two numbers, however, are inconsistent in a broader range of star formation rates. The detected numbers are higher than the expected numbers for galaxies in groups SFRU, SFRA, SFRB, SFRC, and SFRD with star formation rates $\leq 0.4\ M_\odot\ \mathrm{yr}^{-1}$, and lower for galaxies in groups SFRG and SFRH with star formation rates $\geq 5\ M_\odot\ \mathrm{yr}^{-1}$. The detected ULXs, however, follow closely the changes of the surveyed blue light over the whole range of star formation rates in the survey, leading to an approximately linear relation between the two and an almost constant ULX rate per $10^{10}\ L_\odot$ (Fig. 12).

4. SPATIAL DISTRIBUTION OF ULXS

To study the spatial distribution of ULXs and how ULXs trace the blue light, we study the ULX populations in elliptical annuli of the survey galaxies. For each galaxy, the area within $2D_{25}$ is divided into 20 elliptical annuli in steps of $0.1R_{25}$, with R_{25} as the elliptical radius of the D_{25} isophote. For a group of galaxies, we construct 20 ULX populations, with each extracted from the annuli of the same elliptical radius range. For each ULX population, the contamination and the surveyed blue light curve are calculated excluding the $10''$ nuclear region as described in § 2.

The radial distributions are calculated for the ULXs in early-type and late-type galaxies, and compared to the distribution of predicted false ULXs. For the early-type galaxies, these two distributions are consistent with each other (Fig. 14) at a 99.6% confidence level as quantified by a Kolmogorov-Smirnov test. For the late-type galaxies, the radial distribution of detected ULXs shows a peak around $0.5R_{25}$, and is different from the distribution of false ULXs (Fig. 15). A Kolmogorov-Smirnov test shows that the two radial distributions can be the same only at a 2.2×10^{-9} probability level.

A significant concentration of ULXs toward galactic centers is present in the late-type galaxies, as shown by the surface number density of ULXs with the predicted false ULXs subtracted (Fig. 16). There are 79 detected ULXs, 15.7 predicted false ULXs, and 63.3 "true" ULXs within the D_{25} isophotes (Table 2), while there are 60 detected ULXs, 43.1 false ULXs, and 16.9 "true" ULXs between $1D_{25}$ and $2D_{25}$. The bulk of the "true" ULXs (∼80%) is within the D_{25} isophotes, which justifies

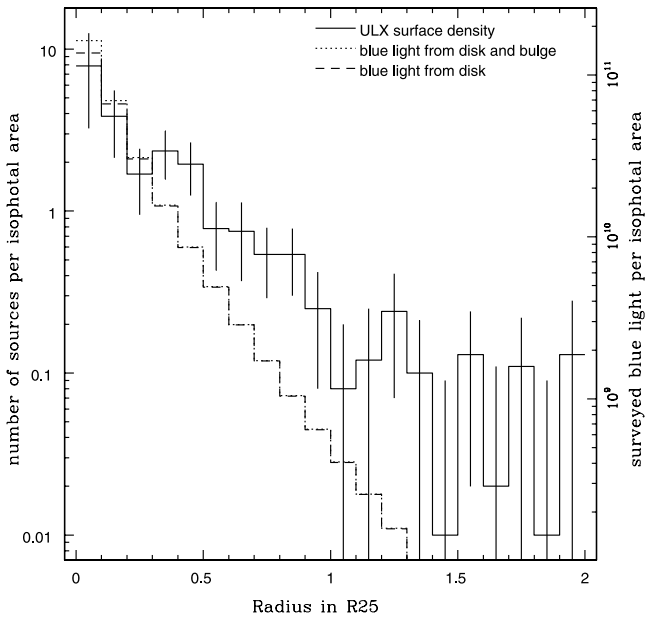

FIG. 16.—Radial distribution of the surface number density of ULXs (*solid line*) in the late-type galaxies, and the surface brightness of surveyed blue light, from the disks and bulges (*dotted line*) and from only the disks (*dashed line*). The contaminating sources and the nuclear regions are excluded in the calculation.

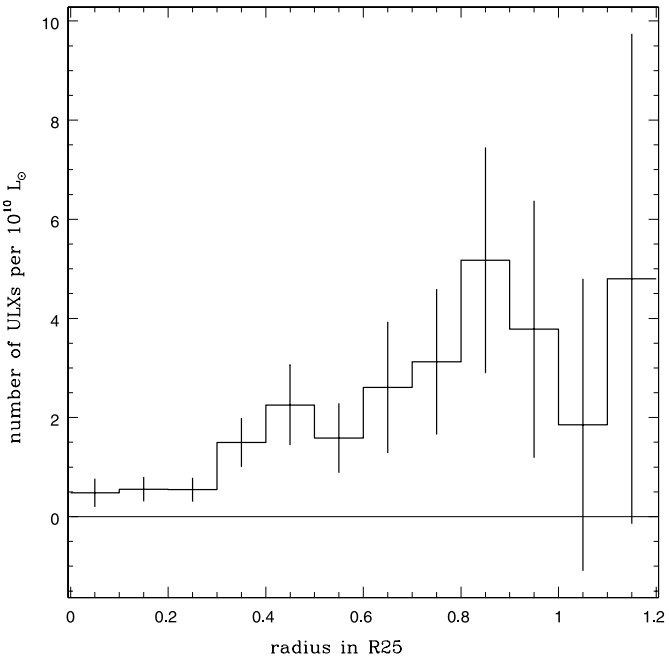

FIG. 17.—Number of ULXs above 10^{39} ergs s^{-1} per unit of surveyed blue light in the late-type galaxies, with the contaminating sources excluded.

our exclusion of ULXs between $1D_{25}$ and $2D_{25}$ in our studies in § 3.

The spatial distribution of ULXs is more extended than the surveyed blue light in the late-type galaxies (Fig. 16). The surveyed blue light, mostly from the disk components, follows an exponential profiles that peaks at $0.3R_{25}$, the average disk scale height. In comparison, the radial distribution of ULXs peaks at $0.5R_{25}$ (Fig. 15). This leads to a gradual increase in the number of ULXs per unit of blue light with radii (Fig. 17), and is consistent with the preferential association of ULXs with the spiral arms that are known to be more extended than the light profile.

The exclusion of a 10″ nuclear region, while devised to exclude the galactic nucleus, leads to a decrease of detected ULXs if ULXs are distributed across the galaxy. The number of excluded ULXs is expected to be small for nearby galaxies ($\leq$5 Mpc) for which the 10″ nuclear region ($\leq$250 pc) corresponds to the bulge without much star formation except in rare occasions. This number increases for distant galaxies, and can be estimated by assuming a constant ratio of ULXs inside and outside a physical radius for galaxies at different distances, which is reasonable given the constant average physical size of galaxies with distances. For example, to estimate the number of excluded ULXs for a galaxy at 30 Mpc, we need to compute the ratio of ULXs inside and outside 10″ (1.5 kpc) from a sample of nearby ULXs, which we take as within 5 Mpc here. For the 81 ULXs in the late-type galaxies between 5 and 40 Mpc, we estimate that 6.3 ULXs in the nuclear regions are excluded based on the spatial distribution of 12 ULXs within 5 Mpc, i.e., the exclusion of nuclear regions decreases the detected ULXs by about 6%. For the starburst/H II galaxies, there are 8 ULXs within 5 Mpc, 33 ULXs between 5 and 40 Mpc, and 3.9 excluded ULXs (10%) in nuclear regions are estimated. Similar method gives 0% (0/14) of excluded ULXs in early-type galaxies. The percentage of excluded ULXs in starburst/H II galaxies is higher than that in average late-type galaxies and that in early-type galaxies, which is expected since ULXs are more concentrated in starburst/H II regions.

5. DISCUSSION

In this paper statistical properties of the ULX populations constructed from our recent HRI survey of X-ray sources in nearby galaxies (Liu & Bregman, 2005) are studied with particular attention to the contamination problem. The ULXs as nonnuclear X-ray point sources above 10^{39} ergs s^{-1} are commonly found in late-type galaxies. For example, ~40% of the late-type galaxies harbor at least one ULX with 0.84 ± 0.13 ULXs per 10^{10} $L_\odot$ in our HRI survey. Here we compare our results to other similar works and discuss the implications for the ULX phenomenon.

5.1. *Comparisons to Similar Works*

Ptak & Colbert (2004) studied the occurrence frequencies of ULXs based on their HRI survey of nearby galaxies within 66.7 Mpc (CP2002). In their survey, they compute the luminosities in 2–10 keV using a power-law spectrum with a photon index of 1.7, and the resultant luminosities are about 1.5 times lower than the luminosities computed in 0.3–8 keV in this survey. They found that the percentage of the survey galaxies that host at least one ULX is 12.3% (28/228) for ULXs above 10^{39} ergs s^{-1}, 7.3% (23/316) for ULXs above 2×10^{39} ergs s^{-1}, 3.1% (14/446) for ULXs above 5×10^{39} ergs s^{-1}, and 1.1% (6/540) for ULXs above 10^{40} ergs s^{-1}. The corresponding occurrence frequencies in this survey are 25% (32/128), 13.7% (27/197), 5.2% (14/270), and 3.1% (9/286), respectively, after considering the luminosity difference. In comparison, this survey, which focuses on the nearby ones within 40 Mpc, shows a significantly higher percentage of galaxies that host low-luminosity ULXs.

Swartz et al. (2004) studied the ULX population in 82 nearby galaxies with *Chandra* ACIS observations. A total of 154 ULX candidates were found in their survey, and there are ~2 ULX candidates per galaxy for both early-type galaxies and late-type galaxies. The number of ULXs per unit (10^{42} ergs s^{-1}) blue luminosity is 0.11 ± 0.02 (0.30 ± 0.11) for early-type (late-type) galaxies, or 0.55 ± 0.10 (1.50 ± 0.55) ULXs per 10^{10} $L_\odot$ given $L_{B\odot} \approx 5 \times 10^{32}$ ergs s^{-1}. These rates are higher than the rates from this HRI survey, especially for early-type galaxies. Swartz et al. calculated the flux in 0.5–8 keV by fitting a power-law model to the spectrum, and corrected for the fitted H I column density that is on average 2×10^{21} cm^{-2}, 10 times higher than the average Galactic H I column density (2×10^{20} cm^{-2}) we used to correct the flux. This leads to luminosities about 1.7 times higher than the luminosities from the HRI survey, and would identify some ordinary LMXBs/HMXBs as ULX candidates and overestimate the ULX rates. In fact, 77 out of 154 ULX candidates in Swartz et al. (including 33 out of 40 ULX candidates in elliptical galaxies) are dimmer than 1.7×10^{39} ergs s^{-1}. Based on a rough comparison of the cumulative luminosity functions of the ULXs to the Chandra Deep Field results they conclude ~14% (44%) of the ULXs in spiral (early-type) galaxies may be background objects. With these low-luminosity ULX candidates removed and the estimated background objects deducted, their ULX rates would be $\sim 0.8 \pm 0.5$ (0.05 ± 0.10) ULXs per 10^{10} $L_\odot$ for spiral (elliptical) galaxies, comparable to our results. The corrected results can also be expressed as $\sim 1.1 \pm 0.7$ (0.2 ± 0.4) ULXs per spiral (elliptical) galaxy.

5.2. *Two Classes of ULXs?*

This HRI survey has significant coverage at low luminosities, with X-ray sources of 2×10^{38} ergs s^{-1} detectable in ~10% of the total surveyed blue light. The luminosity functions, therefore, are studied in the luminosity range of 10^{38}–10^{41} ergs s^{-1},

which enables direct comparisons between the ULX populations and ordinary X-ray binary populations below 10^{39} ergs s^{-1}.

The luminosity function of the X-ray point sources in the early-type galaxies shows a sharp cutoff around 10^{39} ergs s^{-1} in the deep survey (Fig. 5). Such a cutoff has been verified with *Chandra* observations of nearby elliptical galaxies M87, M49, and NGC 4697 (Jordán et al. 2004). The cutoff leads to a rather low ULX rate of -0.13 ± 0.09 ULX per $10^{10}\,M_{\odot}$ for early-type galaxies, and ≤ 0.2 ULX per $10^{10}\,M_{\odot}$ even after allowance for a 20% error in the false ULXs due to background contamination. This cutoff indicates that the ULXs in ellipticals have low luminosities, as suggested by Irwin et al. (2004). For example, all seven ULX candidates in ellipticals in Swartz et al. (2004) are below $\sim 2 \times 10^{39}$ ergs s^{-1}. Since the X-ray sources are dominated by LMXBs due to the lack of the young stellar population in early-type galaxies, the few ULXs in early-type galaxies must be an extension of the ordinary LMXBs.

The luminosity function of the X-ray point sources in the late-type galaxies can be fitted by a single power law between 2.5×10^{38} and 10^{40} ergs s^{-1}, with no changes in the slope or the normalization around 10^{39} ergs s^{-1} between the ULX population and the ordinary X-ray binary populations (Fig. 6). The absence of changes between the ordinary X-ray binaries and the ULXs suggests that the ULXs below 10^{40} ergs s^{-1} must be the high-luminosity extension of the ordinary X-ray binary populations, all of which are associated with the same underlying distributions of stellar mass black holes, binary properties, and accretion rates. This luminosity function is consistent with the universal luminosity function for the X-ray sources (mainly HMXBs) derived from *Chandra* observations of 12 nearby starburst galaxies, as well as the Milky Way and Magellanic Clouds (Grimm et al. 2003), in that both show a similar power-law slope ($\sim$1.7), and no breaks around 10^{39} ergs s^{-1}.

There exists a significant gap around 10^{40} ergs s^{-1} in the luminosity function that signifies a possible cutoff to the ULX extension of the ordinary X-ray binary population (Fig. 6). The deficit of ULXs in this gap is more than accountable with the $3\,\sigma$ error of the power-law fit, and the probability for it to be a Poisson fluctuation is only 1.1%. This cutoff, also present in the work of Grimm et al. (2003), suggests a cutoff of $\sim 100\,M_{\odot}$ in the mass distribution of black holes if the ULXs radiate at the canonical Eddington luminosity. If the mass distribution of black holes cuts off around $\sim 15\,M_{\odot}$, the most massive black hole achievable in the ordinary stellar evolution models, the ULXs must radiate at more than 6 times the Eddington luminosity. The apparent super-Eddington radiation can result from many effects, such as beamed emission (King et al. 2001), emission of a jet (Kording et al. 2002), emission from a supercritical accretion disk (Shakura & Sunyaev 1973), or emission from a magnetized accretion disk where the photon-bubble instabilities operate (Begelman 2002).

The extreme ULXs beyond the gap at 10^{40} ergs s^{-1} might be a different class from the ULXs below 10^{40} ergs s^{-1}. The extreme ULXs may have a different slope from the low-luminosity ULXs, although inconclusive for the small numbers of extreme ULXs per bin. Nine extreme ULXs are detected in the late-type galaxies, much less than the expected 17.6 (i.e., 15.0 expected from the power-law fit and 2.6 contaminating sources). The probability for the deficit of extreme ULXs to be a Poisson fluctuation is only 1.0%. The deficit of extreme ULXs is similar to the number of excluded ULXs due to nuclear region exclusion ($\sim$6), but it is unlikely that all the excluded ULXs are extreme ULXs. The extreme ULXs are usually found in star-forming regions, and some have X-ray spectral features of systems with black holes of $\geq 1000\,M_{\odot}$, e.g., the ULX in Holmberg IX (Miller et al. 2004) and the ULX in NGC 1313 (Miller et al. 2003). Therefore, it is reasonable to suggest that the extreme ULXs are the intermediate-mass black holes, as suggested by Colbert & Mushotzky (1999), while the regular ULXs as an extension of ordinary HMXBs/LMXBs are systems of stellar mass black holes. There are, however, only a few extreme ULXs detected in the HRI survey, and larger surveys with more extreme ULXs are needed to confirm whether they are a truly different class, and study the details of its luminosity function.

5.3. *Young and Old ULX Populations*

A close connection between ULXs and star formation has been revealed by recent optical observations with the *Hubble Space Telescope* (*HST*) and ground-based telescopes. Pakull & Mirioni (2002) observed 15 ULXs in 11 galaxies, and found 13 ULXs associated with well-defined H II regions and emission nebulae. With the superb spatial resolution and sensitivity of *HST*, some ULXs have been identified to young massive stars in star-forming regions, e.g., the ULX in M81 to an O8 V star (Liu et al. 2002b), the ULX in NGC 5204 to a B0 Ib supergiant (Liu et al. 2004), the ULX in Holmberg II to a young star with spectral type between O4 V and B3 Ib (Kaaret et al. 2004), the ULX in NGC 1313 to a star of 15–20 $M_{\odot}$ (Zampieri et al. 2004), and the ULX in NGC 4559 to four young supergiants (Soria et al. 2005). In comparison, only a few ULXs are reported to associate with globular clusters, e.g., the ULX in NGC 4565 (Wu et al. 2002), and the two ULXs in NGC 1399 (Angelini et al. 2001).

This HRI survey lends statistical support to such a connection. This connection implies that ULXs preferentially occur in late-type galaxies than in early-type galaxies owing to the lack of star formation in the latter. In the deep survey, there are 0.72 ± 0.10 ULXs per survey galaxy for the late-type galaxies, while only 0.02 ± 0.10 ULXs per survey galaxies for the early-type galaxies. In late-type galaxies, ULXs preferentially occur on the thin spiral arms or dust lanes, the major sites of star formation, with 75% (81/106) of the ULXs in the clean sample of Paper I in such regions. Among late-type galaxies, the ULX rate for the starburst/H II galaxies with significant current star formation activities (1.50 ± 0.29 ULXs per $10^{10}\,L_{\odot}$) is much higher than for the nonstarburst galaxies (0.57 ± 0.13 ULXs per $10^{10}\,L_{\odot}$). This close connection is also supported by a general increasing trend of the occurrence frequencies and ULX rates with the star formation rate.

The ULXs associated with star formation may be young HMXB systems undergoing thermal timescale mass transfer through Roche lobe overflow with accretion rates high enough to power radiation at near- or even super-Eddington luminosities (King 2002). If all ULXs are the high-luminosity extension of the HMXBs with luminosities above 10^{39} ergs s^{-1}, a linear relation between the number of ULXs and the star formation rate would be expected, because the HMXBs, with a short lifetime ($\sim 10^7$ yr), are an indicator for the current star formation, and their luminosity function is linearly proportional to the star formation rate (Grimm et al. 2003). This linear relation is supported in the HRI survey for galaxies with star formation rates between 1 and $5 M_{\odot}$ yr^{-1}, the same range for most (9/12) of the galaxies Grimm et al. (2003) used to derive the universal luminosity function for the HMXB population, and a linear relation $N_{\rm ULX} = \beta \rm SFR$ ($\beta = 0.85$ for ULXs above 10^{39} ergs s^{-1}). There is, however, a close match between the changes of the detected ULXs and the surveyed blue light over the whole range of star formation rates from ≤ 0.01 to $\sim 10\,M_{\odot}$ yr^{-1} (Fig. 13), leading to an approximately linear relation between the two. This suggests

that the star formation is not the sole determinant, and the blue light is also an (even more) important determinant of the ULX phenomenon.

The HRI survey shows significant deviation from the linear $N_{\rm ULX}$-SFR relation for galaxies with much lower or higher star formation rates. At lower star formation rates ($\leq 0.4\ M_\odot$), the detected ULXs are significantly higher than predicted by the linear relation (Fig. 13), and the extra ULXs must be an extension of LMXBs, which could be soft X-ray transients in their bright outburst phases, as suggested by King (2002). At higher star formation rates ($\geq 5\ M_\odot$, groups SFRG SFRH), the detected ULXs are up to 5 times lower than the prediction (Fig. 13). The deficit of detected ULXs may be alleviated if the 60 μm emission overestimates the star formation rate for galaxies in groups SFRG and SFRH, as in the early-type galaxies or galaxies with AGNs, which can radiate very luminous infrared emission that is not related to star formation activities. Indeed, AGNs are present in 9 out of the 19 galaxies in group SFRH. Another possible way to reduce the detected ULXs is the source blending in the HRI observations for the much larger PSF as compared to *Chandra* observations. The galaxies with the highest SFRs are investigated to estimate the source blending problem in the most severe situation. For 21 such galaxies with *Chandra* observations, there are 16 ULXs detected in *ROSAT* HRI observations, and two of them are resolved into multiple (two) sources in *Chandra* observations. This suggests the source blending may reduce the detected number of ULXs by $\sim$10%, unable to account for the difference between detections and predictions. The deficit of ULXs in groups SFRG and SFR undermines the applicability of the linear relation at high star formation rates ($\geq 5\ M_\odot\ {\rm yr}^{-1}$), which relies on only two peculiar galaxies (NGC 3256 and the Antennae) in Grimm et al. (2003).

Thus, the HRI survey suggests two populations of ULXs, as also suggested by the study of X-ray point source populations with *Chandra* observations (Colbert et al. 2004). One population is the young ULXs associated with the current star formation and the young stellar population, another the old ULXs associated with the old stellar population. The relative percentage of the young and old ULX populations can be estimated with this survey. The ULXs in early-type galaxies, mostly below 2×10^{39} ergs s^{-1}, are necessarily an extension of LMXBs, with a ULX rate of $\leq$0.2 ULX per $10^{10}\ M_\odot$. If the LMXB population in the late-type galaxies has the same luminosity function and thus leads to a similar ULX rate for the old ULX population, the young ULX population must be responsible for $\geq$70% of the ULXs, and for the majority of the ULXs above $\sim 2 \times 10^{39}$ ergs s^{-1} in the late-type galaxies. This is comparable to the results of Colbert et al. (2004), who found 15%–25% of the ULXs in mergers/irregulars and spirals are old ULXs.

We would like to acknowledge the use of NED, HEASARC, SIMBAD, and VizieR services, without which this would not have been possible. We gratefully acknowledge support for this work from NASA under grants NAG5-10765 and HST-GO-09073.

REFERENCES

Angelini, L., Loewenstein, M., & Mushotzky, R. F. 2001, ApJ, 557, L35
Bauer, F. E., Brandt, W. N., Sambruna, R. M., Chartas, G., Garmire, G. P., Kaspi, S., & Netzer, H. 2001, AJ, 122, 182
Begelman, M. C. 2002, ApJ, 568, L97
Bell, E., & de Jong, R. 2001, ApJ, 550, 212
Colbert, E. J. M., & Mushotzky, R. F. 1999, ApJ, 519, 89
Colbert, E., Heckman, T., Ptak, A., & Strickland, D. 2004, ApJ, 602, 231
Colbert, E., & Ptak, A. 2002, ApJS, 143, 25 (CP2002)
de Vaucouleurs, G., de Vaucouleurs, A., Corwin, H., Buta, R., Paturel, G., & Fouqué, P. 1991, Third Reference Catalogue of Bright Galaxies (Berlin: Springer)
Fabbiano, G. 1989, ARA&A, 27, 87
Gao, Y., Wang, Q., Appleton, P., & Lucas, R. 2003, ApJ, 596, L171
Graham, A. 2001, AJ, 121, 820
Grimm, H., Gilfanov, M., & Sunyaev, R. 2003, MNRAS, 339, 793
Hasinger, G., Burg, R., Giacconi, R., Schmidt, M., Trumper, J., & Zamorani, G. 1998, A&A, 329, 482
Irwin, J., Bregman, J., & Athey, A. 2004, ApJ, 60, L143
Jordán, A., et al. 2004, ApJ, 613, 279
Kaaret, P., Ward, M., & Zezas, A. 2004, MNRAS, 351, 83
Kilgard, R., Kaaret, P., Krauss, M., Prestwich, A., Raley, M., & Zezas, A. 2002, ApJ, 573, 138
King, A. R. 2002, MNRAS, 335, 513
King, A. R., Davies, M. B., Ward, M. J., Fabbiano, G., & Elvis, M. 2001, ApJ, 552, L109
Kong, A. K. H., Di Stefano, R., & Yuan, F. 2004, ApJ, 617, L49
Kording, E., Falcke, H., & Markoff, S. 2002, A&A, 382, L13
Liu, J., & Bregman, J. 2005, ApJS, 157, 59 (Paper I)
Liu, J., Bregman, J., & Irwin, J. 2002a, ApJ, 581, L93
Liu, J., Bregman, J., Irwin, J., & Seitzer, P. 2004, ApJ, 602, 249
Liu, J., Bregman, J., Lloyd-Davies, E., Irwin, J., Espaillat, C., & Seitzer, P. 2005, ApJ, 621, L17
Liu, J., Bregman, J., & Seitzer, P. 2002b, ApJ, 580, L31
Makishima, K., et al. 2000, ApJ, 535, 632
Miller, J., Fabian, A., & Miller, M. 2004, ApJ, 607, 931
Miller, J., Fabbiano, G., Miller, M., & Fabian, A. 2003, ApJ, 585, 37
Pakull, M. W., & Mirioni, L. 2002, preprint (astro-ph/0202488)
Ptak, A., & Colbert, E. 2004, ApJ, 606, 291
Rice, W., Lonsdale, C, Soifer, B., Neugebauer, G., Koplan, E., Lloyd, L., de Jong, T., & Habing, H. 1988, ApJS, 68, 91
Rosa-González, D., Terlevich, E., & Terlevich, R. 2002, MNRAS, 332, 283
Shakura, N., & Sunyaev, R. 1973, A&A, 24, 337
Soria, R., & Motch, C. 2004, A&A, 422, 915
Soria, R., Motch, C., Read, A., & Stevens, I. 2004, A&A, 423, 955
Soria, R., Cropper, M., Pakull, M., Mushotzky, R., & Wu, K. 2005, MNRAS, 356, 12
Strohmayer, T., & Mushotzky, R. 2003, ApJ, 586, L61
Sugiho, M., Kotoku, J., Makishima, K., Kubota, A., Mizuno, T., Fukazawa, Y., & Tashiro, M. 2001, ApJ, 561, L73
Swartz, D., Ghosh, K., Tennant, A., & Wu, K. 2004, ApJS, 154, 519
Wu, H., Xue, S., Xia, X., Deng, Z., & Mao, S. 2002, ApJ, 576, 738
Zampieri, L., et al. 2004, ApJ, 603, 523
Zezas, A., Fabbiano, G., Rots, A., & Murray, S. 2002, ApJS, 142, 239